Forecasting experiments of a dynamical-statistical model of the sea surface temperature anomaly field based on the improved self-memorization principle

Mei Hong[1,2], Xi Chen[1], Ren Zhang[1,2], Dong Wang[3], Shuanghe Shen[2] and Vijay P. Singh[4]

[1] *Institute of Meteorology and Oceanography, National University of Defense Technology, Nanjing 211101, China*

[2] *Collaborative Innovation Center on Forecast and Evaluation of Meteorological Disaster, Nanjing University of Information Science &Technology, Nanjing 210044, China*

[3]*Key Laboratory of Surficial Geochemistry, Ministry of Education; Department of Hydrosciences, School of Earth Sciences and Engineering, Collaborative Innovation Center of South China Sea Studies, State Key Laboratory of Pollution Control and Resource Reuse, Nanjing University, Nanjing 210093, China*

[4]*Department of Biological and Agricultural Engineering, Zachry Department of Civil Engineering, Texas A & M University, College Station, TX 77843, USA*

Corresponding authors address:

1. Xi Chen, Research Centre of Ocean Environment Numerical Simulation, Institute of Meteorology and Oceanography, National University of Defense Technology, Nanjing 211101, China

E-mail: chenxigfkd@163.com

2. Ren Zhang, Research Centre of Ocean Environment Numerical Simulation, Institute of Meteorology and Oceanography, National University of Defense Technology, Nanjing 211101, China

E-mail: 254247175@qq.com

Abstract: With the objective of tackling the problem of inaccurate long-term El Niño Southern Oscillation (ENSO) forecasts, this paper develops a new dynamical-statistical forecast model of sea surface temperature anomaly (SSTA) field. To avoid single initial prediction values, a self-memorization principle is introduced to improve the dynamical reconstruction model, thus making the model more appropriate for describing such chaotic systems as ENSO events. The improved dynamical-statistical model of the SSTA field is used to predict SSTA in the equatorial eastern Pacific and during El Niño and La Niña events. The long-term step-by-step forecast results and cross-validated retroactive hindcast results of time series T_1 and T_2 are found to be satisfactory, with a Pearson correlation coefficient of approximate 0.80 and a mean absolute percentage error (MAPE) of less than 15%. The corresponding forecast SSTA field is accurate in that not only is the forecast shape similar to the actual field, but also the contour lines are essentially the same. This model can also be used to forecast the ENSO index. The temporal correlation coefficient is 0.8062, and the MAPE value of 19.55% is small. The difference between forecast results in spring and those in autumn is not high, indicating that the improved model can overcome the spring predictability barrier to some extent. Compared with six mature models published previously, the present model has an advantage in prediction precision and length, and is a novel exploration of the ENSO forecast method.

Keywords: Dynamical-statistical forecast model; self-memorization principle; sea surface temperature field; long-term forecast of ENSO

1. Introduction

The El Niño Southern Oscillation (ENSO), the well-known coupled atmosphere –ocean phenomenon, was firstly proposed by Bjerknes (1969). The ENSO phenomenon can influence regional and global climates, so the prediction of ENSO has received considerable public interest (Rasmusson and Carpenter, 1982; Glantz et al., 1991).

Over the past two to three decades, one might reasonably expect the ability to predict warm and cold episodes of ENSO at short and intermediate lead times to have gradual improvement (Barnston et al., 2012). Many countries have been focusing on ENSO forecasts since the 1990s, and the ENSO forecast has become one of the important research topics in the International Climate Change and Predictability Research plan. The U.S. International Research Institute for Climate and Society, the U.S. Climate Prediction Centre, Japan Meteorological Agency, and European Centre for Medium-Range Weather Forecasting have developed different coupled atmosphere–ocean models to forecast ENSO (Saha et al., 2006; Molteni et al., 2007, Zheng et al., 2016) .

The forecast models can generally be divided into two types (Palmer et al., 2004, Zheng et al., 2017). The first type is typified by a dynamical model, which mathematically expresses physical laws that govern how the ocean and the atmosphere interact. The second type is typified by a statistical model, which requires a large amount of historical data and analyses the data to do forecasting (Chen et al., 1995; Moore et al., 2006).

Over the past three decades, ENSO predictions have made remarkable progress, reaching a stage where reasonable statistical and numerical forecasts (Jin et al., 2008)can be made 6–12 months in advance (Wang et al., 2009a). . However, there are three problems remaining to be resolved (Zhang et al., 2003a): (1) The current ENSO predictions are mainly limited to the short term, such as annual and seasonal predictions; (2) Although the representation of ENSO in coupled models has been advanced considerably during the last decade, several aspects of the simulated climatology and ENSO are not well reproduced by the current generation of coupled models. The systematic errors in SST are often very large in the equatorial Pacific, and model representations of ENSO variability are often weak and/or incorrectly located (Neelinet al. 1992; Mechoso et al. 1995; Delecluse et al. 1998; Davey et al. 2002). (3) Coupled models of ENSO predictions initialized from observed initial states tend to adjust towards their own climatological mean and variability, leading to forecast errors. The errors associated with such adjustments tend to be more pronounced during boreal spring, which is often called the ‘‘spring predictability barrier’’ (Webster et al., 1999). More efficient models are therefore desired (Belkin and Niyogi, 2003; Weinberger and Saul, 2006). Therefore, the idea of combining dynamical and statistical methods to improve weather and climate prediction has been developed in many studies (Huang et al., 1993;Yu et al., 2014a; Yu et al.,2014b). By introducing genetic algorithms (GAs), Zhang et al. (2006) inverted and reconstructed a new dynamical-statistical forecast model of the tropical Pacific sea surface temperature (SST) field using historic statistical data (Zhang et al., 2008). However,

there is one flaw in the forecast model: the time-delayed SST field. It is because that ENSO is a complicated system with many influencing factors. To overcome information insufficiency in the forecast model, Hong et al. (2014) selected the tropical Pacific SST, SSW and SLP fields as three modelling factors and utilized the GA to optimize model parameters.

However, the above dynamical prediction equations which were ,proposed by Hong et al.(2014), greatly depend on a single initial value, creating long-term forecasts over 8 months that diverged significantly. These unsatisfactory results indicate that this model needs to be improved. Cao (1993) first proposed the self-memorization principle, which transforms the dynamical equations with the self-memorization equations, wherein the observation data can determine the memory coefficients. This method has been widely used in forecast problems in environmental, hydrological and meteorological fields (Feng et al., 2001; Gu, 1998; Chen et al., 2009). The method can avoid the question of initial conditions for the differential equations, so it can be introduced here to improve the proposed dynamical forecast model.

Therefore, an improved dynamical-statistical forecast model of the SST field and its impact factors with a self-memorization function was developed. The improved model can absorb the information from past observations.

This paper is organized as follows: Research data and forecast factors are introduced in section 2. In Section 3 the reconstruction of the dynamical model of SSTA field is described. To improve the reconstruction model, the self-memorization

principle is introduced in Section 4. Model forecast experiments are described in Section 5, and conclusions are given in Section 6.

2. Research data and forecast factors

2.1 Data

The monthly average SST data were obtained from the UK Met Office Hadley Centre for the region (30°S-30°N; 120°E-90°W). The gridded 1° × 1° Met Office Hadley Sea Ice and SST dataset (HadISST1; Rayner et al. 2003) includes both in situ and available satellite data. The sea areas provide important information on ocean-atmosphere coupling in the East and West Pacific Ocean and the El Niño /La Niña events. The reanalysis data, zonal winds and sea level pressures were obtained from the National Center for Environmental Forecast of America and the National Center for Atmospheric Research (Kalnay et al., 1996). The sea surface height (SSH) field was obtained from Simple Ocean Data Assimilation (SODA) data (James and Benjamin, 2008). Outgoing longwave radiation (OLR) was obtained from the National Oceanic and Atmospheric Administration (NOAA) satellites, at a resolution of 0.5° × 0.5°(Liebmann and Smith, 1996).The Southern Oscillation Index (SOI) data were obtained from the Climate Prediction Center (CPC). The time series of all data were from Jan. 1951 to Dec. 2010, 720 months in total.

2.2 EOF deconstruction

The sea surface temperature anomaly (SSTA) field can be calculated from the SST field and can be deconstructed into time (coefficients)-space (structure) using the empirical orthogonal function (EOF) method. Detailed information on the EOF

method can be seen in the related references (Dommenget & Latif, 2002). We have used covariance matrix，because the covariance matrix was selected to diagnose the primary patterns of co-variability in the basin-wide SSTs, rather than the patterns of normalized covariance (or correlation matrix).

We used the smooths function with MATLAB to smooth the SSTA field before the EOF deconstruction, which is five points two times moving, mainly filtering out some noise points and outliers. Then an EOF analysis of smoothed anomalies was performed, and the first two SSTA EOFs are shown in Figs. 1a and 1c. The principal component (PC) time series corresponding to the first and second EOFs are shown in Figs. 1b and 1d. The first EOF pattern, which accounted for 61.33% of the total SSTA variance, represented the mature ENSO phase (El Niño or La Niña), and the corresponding PC time series was highly correlated (with a correlation coefficient of 0.85) with the cold tongue index (SST anomaly averaged over 4 °S–4 °N, 180 °–90 ° W) over the whole period. The second EOF, accounting for 14.52% of the total SSTA variance, indicated the ENSO signal beginning to enhance. Compared with the first mode, these were slightly attenuated in terms of the scope and intensity. The above analysis is similar to the EOF analysis of the SSTA field in the previous studies (Johnson et al., 2000;Timmermann et al., 2001). This indicates that the front two variance contribution modes can describe the main characteristics of the SSTA field and El Niño/La Niña. Therefore, we can choose the T_1, T_2 time series EOF decomposition modes as the modelling objects.

2.3 Selection of other prediction model factors

158 Considering the complexity of computation, the amount of variables in the
159 equations of our model can't be too large, usually 3 or 4 for the best. This has been
160 explained in our previous studies (Zhang et al., 2006; Zhang et al., 2008). If there are
161 more than 4 variables in the modeling equation, it will cause the amount of
162 parameters such as $a_1, a_2, ...a_n, b_1, b_2, ...b_n, ...$ too large. The huge computation makes it
163 difficult to be precisely modeled. Thus, the total number of parameters in the model of
164 five variables was 102, which may cause an overfitting problem. Hence, when we
165 selected the model of five or six variables which entailed large amounts of
166 computation that made precision difficult, and too many parameters might cause an
167 overfitting phenomenon. If we choose only two or even fewer variables, the forecast
168 performance is poor too. Too few variables cause too small reconstructed parameters,
169 resulting in amounts of important information missing out in the model. Thus, four
170 variables are best for dynamically and accurately modeling. Because we have chosen
171 two time series in section2.2 as the modeling objects, now we should select the other
172 two ENSO intensity impact factors.

173 The ENSO intensity impact factor is an important issue in ENSO prediction.
174 Previous studies have been completed in this area, which found that teleconnection
175 patterns, temperature, precipitation, wind and SSH may affect ENSO strength. For
176 example, Trenberth et al. (1998) noted that PNA, SOI and OLR in the Pacific
177 Intertropical Convergence Zone (ITCZ) are all closely related to ENSO.
178 Webster(1999) pointed out after the 1970, Indian Ocean dipole (IOD) is not only
179 affected by ENSO, but also affected the strength of ENSO (Ashok et al., 2001). Yoon

and Yeh (2010) reported that the Pacific Decadal Oscillation (PDO) disrupts the linkage between El Ni˜no and the following Northeast Asian summer monsoon (NEASM) through inducing the Eurasian pattern in the mid-high latitudes. The vast majority of studies (Tomita and Yasunari, 1996; Zhou and Wu, 2010; Kim et al., 2017) have concentrated on the impacts of ENSO on the East Asian winter monsoon(EAWM). During the EAWM season, ENSO generally reaches its mature phase and has the most prominent impact on the climate. Wang et al. (1999a) and Wang et al. (1999b) suggested that the zonal wind factors in the eastern and western equatorial Pacific play a critical role in the phase of transition of the ENSO cycle, which could excite eastward propagating Kelvin waves and affect the SSTA in the equatorial Pacific. Zhao et al. (2012) analyzed the characteristics of the tropical Pacific SSH field and its impact on ENSO events.

Based on the above analysis, we have selected nine factors, which may be closely related with the ENSO index (Niño3.4).

(1)The zonal wind in the eastern equatorial Pacific factor (u1) was calculated as the grid-point average of zonal wind in the area [5 °S ~ 5 °N, 150 °W ~ 90 °W].

(2) The zonal wind in the western equatorial Pacific factor (u2) was calculated as the grid-point average of zonal wind in the area [0 °~ 10 °N; 135 °E ~ 180 °E].

(3) The PNA teleconnection factor was obtained from the CPC.

(4) the dipole mode index factor (DMI) was obtained from SSTA for June-July-August (JJA) based on Saji(1999) method.

(5) The SOI factor was obtained from the CPC.

(6) The PDOI factor was obtained from department of Atmospheric Sciences in the university of Washington. The web is http://tao.atmos.washinton.edu/pdo/RDO.latest.

(7) The EAWM index (EAWMI) factor was proposed by Yang et al. (2002), which is defined by the meridional 850-hPa winds averaged over the region (20 °~40 °N, 100 °~140 °E).

(8) The OLR in the ITCZ factor was calculated as the grid-point average of OLR in the area [10 °N～20 °N，120 °E～150 °E].

(9) The SSH factor was calculated as the grid-point average of the SSH data in the area [10 °S ~ 10 °N; 120 °E ~ 60 °W].

A correlation analysis of the above factors was carried out and the results are shown in Table 1.

Table 1 shows that SOI and EAWMI have the stronger correlation with the front two time series T_1, T_2 than the other 7 factors. The results are also consistent with previous research (Clarke and Van Gorder, 2003; Drosdowsky, 2006; Zhang et al., 1996; Wang et al., 2008; Yang and Lu, 2014). Therefore, the first time series T_1, the second time series T_2, SOI and EAWMI will be selected as prediction model factors.

3. Reconstruction of dynamical model based on GA

Takens' delay embedding theorem (Takens, 1981) provides the conditions under which a smooth attractor can be constructed from observations made with a generic function. Later results replaced the smooth attractor with a set of arbitrary box-counting dimensions and the class of generic functions with other classes of

functions. Takens had shown that if we measured any single variable with sufficient accuracy for a long period of time, it would be possible to construct the underlying dynamical structure of the entire system from the behavior of that single variable using delay coordinates and the embedding procedure. It was therefore possible to construct a dynamical model of system evolution from the observed time series. Introducing this idea here, four time series of the T_1, T_2, SOI and EAWMI factors were chosen to construct the dynamical model.

The basic idea of statistical-dynamical model construction is discussed in Appendix A and was introduced in our previous work (Zhang et al., 2006; Hong et al., 2014).

A simplified second-order nonlinear dynamical model can be used to depict the basic characteristics of atmosphere and ocean interactions (Fraedrich, 1987). Suppose that the following nonlinear second-order ordinary differential equations are taken as the dynamical model of reconstruction. In the equations, x_1, x_2, x_3, x_4 were used to represent the time coefficient series of T_1, T_2, SOI and EAWMI.

$$\begin{aligned}
\frac{dx_1}{dt} &= a_1x_1 + a_2x_2 + a_3x_3 + a_4x_4 + a_5x_1^2 + a_6x_2^2 + a_7x_3^2 + a_8x_4^2 + a_9x_1x_2 + a_{10}x_1x_3 + a_{11}x_1x_4 + a_{12}x_2x_3 + a_{13}x_2x_4 + a_{14}x_3x_4 \\
\frac{dx_2}{dt} &= b_1x_1 + b_2x_2 + b_3x_3 + b_4x_4 + b_5x_1^2 + b_6x_2^2 + b_7x_3^2 + b_8x_4^2 + b_9x_1x_2 + b_{10}x_1x_3 + b_{11}x_1x_4 + b_{12}x_2x_3 + b_{13}x_2x_4 + b_{14}x_3x_4 \\
\frac{dx_3}{dt} &= c_1x_1 + c_2x_2 + c_3x_3 + c_4x_4 + c_5x_1^2 + c_6x_2^2 + c_7x_3^2 + c_8x_4^2 + c_9x_1x_2 + c_{10}x_1x_3 + c_{11}x_1x_4 + c_{12}x_2x_3 + c_{13}x_2x_4 + c_{14}x_3x_4 \\
\frac{dx_4}{dt} &= d_1x_1 + d_2x_2 + d_3x_3 + d_4x_4 + d_5x_1^2 + d_6x_2^2 + d_7x_3^2 + d_8x_4^2 + d_9x_1x_2 + d_{10}x_1x_3 + d_{11}x_1x_4 + d_{12}x_2x_3 + d_{13}x_2x_4 + d_{14}x_3x_4
\end{aligned} \tag{1}$$

Based on the parameter optimization search method of GA in Appendix A, the

time coefficient series of T_1, T_2, SOI and EAWMI from January 1951 to April 2008 are chosen as the expected data to optimize and retrieve model parameters. In order to eliminate the dimensionless relationship between variables, data standardization $x_{nor} = \frac{x - x_{\min}}{x_{\max} - x_{\min}}$ is to transform data from different orders of magnitude to the same order of magnitude. Finally, we made forecast results revert back to the raw data magnitude by $x = x_{nor}(x_{\max} - x_{\min}) + x_{\min}$.

In order to quantitatively compare the relative contribution of each item of our model to the evolution of the system, we calculated the relative variance contribution. The formula is as follows: $R_i = \frac{1}{n}\sum_{j=1}^{n}[\frac{T_i^2}{\sum_{i=1}^{14} T_i^2}], i = 1,2,...,14$, Where n is the length of the data, $T_i = a_1x_1, a_2x_2, ..., a_{14}x_3x_4$ is the item in the equation. According to our previous research (Hong et al., 2007), the variance contribution of the real item reflecting the performance of the model has a large proportion, while the variance contribution of the false term is almost zero, so we delete the weak items of $R_i < 0.01$.

After deleting the weak items, the nonlinear dynamical model of the first time series T_1, the second time series T_2, SOI and EAWMI can be reconstructed as follows:

$$
\begin{aligned}
\frac{dx_1}{dt} &= F_1 = -0.3328x_1 + 1.2574x_2 - 0.3511x_3 - 0.0289x_1^2 + 3.1280x_3^2 + 0.0125x_1x_2 + 2.7805x_1x_3 - 1.5408x_2x_4 \\
\frac{dx_2}{dt} &= F_2 = 1.0307x_1 - 3.1428x_2 + 0.3095x_4 + 4.2301x_1^2 - 1.2066x_2^2 + 2.5024x_4^2 - 0.2891x_1x_3 + 0.7815x_1x_4 - 0.4266x_3x_4 \\
\frac{dx_3}{dt} &= F_3 = -2.3155x_1 + 3.2166x_3 + 1.5284x_4 - 1.4527x_2^2 - 0.0034x_3^2 - 4.1206x_4^2 - 0.0025x_1x_4 + 0.0277x_2x_3 + 1.2860x_2x_4 \\
\frac{dx_4}{dt} &= F_4 = 0.4478x_2 - 0.0268x_4 + 0.8995x_1^2 - 2.3890x_3^2 + 0.2037x_4^2 + 1.3035x_1x_2 + 2.0458x_1x_4 - 2.0015x_2x_4
\end{aligned}
\tag{2}
$$

The model required testing. Because the training period was from January 1951

to April 2008, we chose T_1, T_2,SOI and EAWMI of May 2008, which were not used as initial forecast data in the modeling. Next, the Runge–Kutta method was used to do the numerical integration of the above equations, and every step of the integration was regarded as 1 month's worth of forecasting results. As a result, forecast results of four time series over a period of 20 months were obtained. Here, the focus was on the forecast results of T_1 and T_2, as shown in Fig.2.

The pearson correlation coefficient (CC) (Wang et al. 2009b) and the mean absolute percentage error (MAPE)(Hu et al. 2001) are employed as objective functions to calibrate the model. The CC evaluates the linear relationship between the observed and predicting values and MAPE measures the difference between the observed and predicting values.

From Fig. 2, forecast performance of T_1 and T_2 within 5 months was better. Using T_1 as an example, the CC between model predictions and corresponding observations over the first five months forecasts was 0.8966 and MAPE was 8.32%. However, after 5 months, MAPE increased rapidly, and was 31.29% at 10 months. The model forecast then significantly diverged from observations, and the forecast became inaccurate. After 10 months, the forecast results became increasingly worse, which indicated that the forecast of the model after 5 months was unacceptable. The forecast results of T_2 were similar to those of T_1.

The model's skill should be further assessed by cross-validated retroactive hindcasts of the time series. As in the above example, omitting a portion of the time series (12 months, Jan. 1951 to Dec. 1951) from observations, we trained the model

based on the data from Jan. 1951 to Dec. 2010, and then predicted the omitted segments (12 months, Jan. 1951 to Dec. 1951). Then in the next prediction experiment, the omitted segment is Jan.1952 to Dec. 1952 and the training samples are Jan. 1951 to Dec.1951 and Jan.1953 to Dec.2010. So the forecast time series is Jan.1952 to Dec. 1952.We then repeated this procedure by moving the omitted segment along the entirety of the available time series. Each experiment has used the different training sample and established the different model equation (but the method is the same). The similar process of the cross-validated retroactive hindcasts has also been used in the previous literatures (Hu et al., 2017).

Finally, we obtained cross-validated retroactive hindcast results of T_1 and T_2, as shown in Fig. 3. So the forecast results of 60 cross experiment (each experiment is the prediction of the 12 month as Fig.2) according to the time sequence can merger into a new time series (from Jan.1951-Dec.2010), and then CC and MAPE can be calculated by the new prediction time series and the time series of the actual value. Figure 3 is combined results of the 60 forecast experiments.

As Fig. 2, the forecast performance of T_1 and T_2 in Fig. 3 was not satisfactory. The model forecast significantly diverged from observations, and the forecast became inaccurate. The CC of T_1 and T_2 between model predictions and corresponding observations were 0.3411 and 0.4176, respectively. Additionally, the MAPE of T_1 and T_2 were 65.42% and 57.56%, respectively. This indicates that the forecast of the model in the long -term was inaccurate and unacceptable.

The forecast result may be inaccurate when the integral forecasting time is long. There will be a significant divergence which will cause an ineffective forecast. To

improve the forecast accuracy, the forecast not only depends on the integral equation but also on a single initial value. Choosing the different initial value will cause different forecast accuracy. For example, in a total of 60 cross-validated retroactive hindcasts examples, the minimum MAPE was 37.65%, while the maximum MAPE was 89.88%. A forecast, depending on a single initial value, will cause instability of the forecast results. These two problems are addressed by introducing the self-memorization principle in the next section.

4. Introduction of self-memorization dynamics to improve the reconstructed model

In the above discussion, it was shown that the accuracy of the forecast results of equation (2) were unsatisfactory. To improve long-term forecasting results, the principle of self-memorization can be introduced into the mature model (Gu, 1998; Chen et al., 2009). The principle of self-memorization dynamics (Cao, 1993; Feng et al., 2001) can be seen in Appendix B.

Based on Eq. (B10) in Appendix B, the improved model can be expressed as follows:

$$\begin{cases} x_{1t} = \sum_{i=-p-1}^{-1} \alpha_{1i} y_{1i} + \sum_{i=-p}^{0} \theta_{1i} F_1(x_{1i}, x_{2i}, x_{3i}, x_{4i}) \\ x_{2t} = \sum_{i=-p-1}^{-1} \alpha_{2i} y_{2i} + \sum_{i=-p}^{0} \theta_{2i} F_2(x_{1i}, x_{2i}, x_{3i}, x_{4i}) \\ x_{3t} = \sum_{i=-p-1}^{-1} \alpha_{3i} y_{3i} + \sum_{i=-p}^{0} \theta_{3i} F_3(x_{1i}, x_{2i}, x_{3i}, x_{4i}) \\ x_{4t} = \sum_{i=-p-1}^{-1} \alpha_{4i} y_{4i} + \sum_{i=-p}^{0} \theta_{4i} F_4(x_{1i}, x_{2i}, x_{3i}, x_{4i}) \end{cases} \quad (3)$$

where y_i is replaced by the mean of two values at adjoining times; i.e., $y_i \equiv \frac{1}{2}(x_{i+1} + x_i)$; F is the dynamical core of the self-memorization equation, which

326 can be obtained from Eq. (2); and α and θ are the memory coefficients, the formula

327 for which can be found in Appendix B.

328 If the values of α and θ can be obtained, Eq. (3) can be used to obtain the

329 results of final prediction. The memory coefficients α and θ in Eq. (3) were

330 calibrated using the least-squares method with the same data (January 1951 to April

331 2008) as those used in Section 3. Eq. (3) can be deconstructed as follows (M is the

332 length of the time series):

333
$$X=\begin{bmatrix} x_{11} \\ x_{12} \\ . \\ . \\ . \\ x_{1\mathrm{M}} \end{bmatrix}, \alpha=\begin{bmatrix} \alpha_{-p-1} \\ \alpha_{-p} \\ . \\ . \\ . \\ \alpha_{-1} \end{bmatrix}, Y=\begin{bmatrix} y_{-p-1,1} & y_{-p,1} & \cdots & y_{-1,1} \\ y_{-p-1,2} & y_{-p,2} & \cdots & y_{-1,2} \\ . & . & & . \\ . & . & & . \\ . & . & & . \\ y_{-p-1,\mathrm{M}} & y_{-p,\mathrm{M}} & \cdots & y_{-1,M} \end{bmatrix}, \Theta=\begin{bmatrix} \theta_{-p} \\ \theta_{-p+1} \\ . \\ . \\ . \\ \theta_0 \end{bmatrix},$$

334
$$F=\begin{bmatrix} F_{-p,1} & F_{-p+1,1} & \cdots & F_{0,1} \\ F_{-p,2} & F_{-p+1,2} & \cdots & F_{0,2} \\ . & . & & . \\ . & . & & . \\ . & . & & . \\ F_{-p,M} & F_{-p+1,\mathrm{M}} & \cdots & F_{0,\mathrm{M}} \end{bmatrix}$$

335 The matrix equation is:

336
$$X=Y\alpha+F\theta \qquad (4)$$

337 where $Z=[Y\vdots F]$, $W=\begin{bmatrix} \alpha \\ \vdots \\ \Theta \end{bmatrix}$.

338 Eq. (4) can be written as:

339
$$X=ZW \qquad (5)$$

340 The memory coefficients vector W can be calibrated using the least squares

method:

$$W = (Z^T Z)^{-1} Z^T X \quad (6)$$

The memory coefficients a, θ can be obtained from Eq. (6). We then made a prediction using the self- memorization equation (3), which used the p values before t_0.

The coefficients in F and W were used with the same training data from January 1951to Apr.il 2008. In the forecast examples, we trained both the coefficients in F and W at the same time, but in the paper we describe them separately to facilitate the reader for better understanding.

5. Model prediction experiments

5.1 Forecast of time series T_1 and T_2

The training sample for the model was from January1951 to April 2008. Here, from Eq. (3), the forecast results using T_1, T_2, SOI and EAWMI factors can be calculated, called as step-by-step forecast.

When the retrospective order p is confirmed, step-by-step forecasts can be carried out. For example, when the T_1, T_2, SOI and EAWMI values of May 2008 were forecast, y_i was obtained from the previous p +1 time of T_1, T_2, the SOI and the EAWMI data, and $F_i(x_{1i}, x_{2i}, x_{3i}, x_{4i})$ was obtained from the previous p times of T_1, T_2, the SOI and the EAWMI data. All four equations were integrated simultaneously. Taking these in Eq. (3), we can get the T_1, T_2, SOI and EAWMI values of May 2008, which these can be taken as the initial values for the next prediction step. Then, the T_1, T_2, SOI and EAWMI values from June 2008 and so on, can be generated.

363 5.1.1 Determination of p

364 Based on the self-memorization principle, the self-memorization of the system
365 determines the retrospective order p (Cao, 1993). If the system forgets slowly,
366 parameters a and θ will be small and the p value should be high. The SSTA field
367 forecasts were on a monthly scale, the change of which was slow in contrast to
368 large-scale atmospheric motion. So parameters a and θ were small, and generally,
369 the p value was in the range 5 to 15(Cao, 1993).

370 The retrospective order p was obtained by a trial calculation method. We selected
371 the p values in the range 4 to 16 to construct the model. The CC and MAPE of
372 long-term fitting test (from February 1951 to December 2010) are shown in Table 2,
373 which can be used as the standard to determine the retrospective order p.

374 Table 2 indicates that when $p = 6$, the MAPE values of long-term fitting test
375 were the smallest and the CCs were the largest. Also, when p from 5 to 9, The CCs
376 were all more than 0.58 and the forecast results were all good, which is consistent
377 with our interpretation of the physical mechanisms in section 6.2 below. SOI and
378 EMWMI were 5-12 months lead relationships with SST (Xu et al., 1993; Chen et al,
379 2010; Wang et al., 2003). Using a cumulative period of SOI, EMWMI 5-8 months
380 ahead as initial values can help improve the final forecast results. Our results in table
381 2 are consistent with the actual physical ENSO process. Therefore, we selected the
382 retrospective order as p=6.

383 Then, the prediction experiments can be carried out, based on improved
384 self-memorization Eq. (3).

385 The improved self-memorization equation of T_1, T_2, SOI and EAWMI can then be
386 established. After the differential equation was discretely dealt with, the memory
387 coefficients were solved by the least-squares method given in section 4 (Training
388 period is January 1951 to April 2008). Finally, the improved prediction equation of
389 T_1, T_2, SOI and EAWMI, based on the self-memorization principle, can be expressed
390 as:

391
$$\begin{cases} x_{1t} = \sum_{i=-7}^{-1} \alpha_{1i} y_{1i} + \sum_{i=-6}^{0} \theta_{1i} F_1(x_{1i}, x_{2i}, x_{3i}, x_{4i}) \\ x_{2t} = \sum_{i=-7}^{-1} \alpha_{2i} y_{2i} + \sum_{i=-6}^{0} \theta_{2i} F_2(x_{1i}, x_{2i}, x_{3i}, x_{4i}) \\ x_{3t} = \sum_{i=-7}^{-1} \alpha_{3i} y_{3i} + \sum_{i=-6}^{0} \theta_{3i} F_3(x_{1i}, x_{2i}, x_{3i}, x_{4i}) \\ x_{4t} = \sum_{i=-7}^{-1} \alpha_{4i} y_{4i} + \sum_{i=-6}^{0} \theta_{4i} F_4(x_{1i}, x_{2i}, x_{3i}, x_{4i}) \end{cases} \quad (7)$$

392 where

393
$$\alpha = [\alpha_{ij}] = \begin{bmatrix} 0.0315 & -2.113 & 0.0284 & 2.1468 & 0.0688 & -0.7014 & 1.3248 \\ 0.4088 & -1.887 & -1.0233 & 1.5485 & 0.9028 & 1.0255 & -0.6443 \\ -0.9088 & -0.2557 & 0.9671 & -0.0054 & 1.0568 & 2.9764 & -0.5234 \\ 0.2088 & -1.0567 & 0.4891 & -0.5066 & -0.4890 & 1.4555 & 1.0966 \end{bmatrix}$$
$(i = 0,1,...,4; \mathrm{j} = -7,-6,...,-1)$

394
$$\theta = [\theta_{ij}] = \begin{bmatrix} 0.0485 & 0.0425 & -1.7688 & 0.8543 & 2.8901 & -0.1788 & -0.9066 \\ 0.07642 & 0.0941 & -1.2466 & -0.2288 & 0.1097 & 2.3221 & -1.4228 \\ -0.5288 & 1.2368 & -0.5568 & -0.0155 & 0.2886 & -0.1560 & 1.2775 \\ 1.5335 & -0.2887 & -0.5336 & -0.6072 & -0.5611 & 1.0225 & -1.0625 \end{bmatrix}$$
$(i = 0,1,...,4; \mathrm{j} = -6,-5,...,0)$

395 The step-by-step forecast was performed. The retrospective order $p = 6$ means
396 that earlier seven observation data ($p + 1 = 7$) should be used during the forecasting
397 process. The forecast results per month were saved for the next period predictions.

398 5.1.2 Long-term step-by-step forecasts of T_1 and T_2

399 To test the actual forecast performance of the above improved model, long-term

400 step-by-step forecasts of T_1 and T_2 from May 2008 to December 2010 for 20 months
401 were carried out, as shown in Fig. 4. The forecast results of T_1 and T_2 were good.
402 Within 8 months, the CCs of T_1 and T_2 were 0.9163 and 0.9187. MAPEs of T_1 and
403 T_2 were small, only 5.86% and 6.78%. The forecast time series from 8 months to 14
404 months gradually diverged, but the trend was acceptable. The CCs of T_1 and T_2
405 reached 0.8375 and 0.8251, and MAPEs of T_1 and T_2 were 8.32% and 9.11%. After
406 14 months, forecast began to diverge and the error started to increase, but the CCs of
407 T_1 and T_2 remained about 0.6899 and 0.6782, and MAPEs reached 18.31% and
408 19.44%, which can be acceptable.

409 **5.2 Cross-validated retroactive hindcasts of time series T_1 and T_2**

410 As in section 3, the model's skill should be further assessed by cross-validated
411 retroactive hindcasts of the time series. Because our step-by-step forecasts need the
412 earlier seven observation data ($p + 1 = 7$), we can obtain cross-validated retroactive
413 hindcast results of T_1 and T_2 from August 1951 to December 2010, as shown in Fig.
414 5.

415 From Fig. 5, the forecast performance of T_1 and T_2 was good. The CCs of
416 T_1 and T_2 were 0.7124 and 0.7036, respectively. The MAPEs of T_1 and T_2 were
417 small, only 19.57% and 19.79%, respectively. The peaks and valleys of T_1 and T_2
418 were also forecasted accurately. The forecast results indicated that the cross-validated
419 retroactive hindcast results of T_1 and T_2 were close to the observed values.
420 Compared to Fig. 3, the improved model had better forecast abilities than the original
421 model.

Many researchers (Zhang et al., 2003b; Smith, 2004) have used Oceanic Niño Index (ONI) which is used by the U.S. NOAA Climate Prediction Center to determine the El Niño and La Niña years. It defined that the ONIs of five consecutive months in winter were all more than 0.5 (less than -0.5) is the ElNiño (La Niña) year. Based on the above criterion, we can divide the total 60 years (1951-2010) into three categories. It includes the 18 examples of ElNiño year (such as 1958, 1964, 1966, etc.), 22 examples of LaNiña year (such as 1951, 1955, 1956, etc.) and the remaining 20 experiments of the neutral year. Since the details in Fig.5 is not clear, we list the forecast results of 60 experiments (including 18 El Niño examples, 22 La Niña examples and 20 Neutral examples) in table 3.

From table 3, the average of CC of both T_1 and T_2 of 60 experiments within 6 months was more than 0.84 and MAPE was less than 8%. The average of CC within 12 months was more than 0.74 and MAPE was less than 12%. According to the literature (Barranel et al., 1999), when MAPE was less than 15%, which means the error was not great and the forecast results were good. Obviously, the forecast results of ElNiño / LaNiña experiments were a little worse than those of neutral examples, which means the forecast ability of our model for the abnormal situation was a little worse than those for the normal situation. But even for ElNiño / LaNiña experiments, the average of CC was still more than 0.7 and MAPE was less than 15%, which means the error was not too large and was still within an acceptable range.

5.3Forecast of the SSTA field

When we obtained the forecast results of the time coefficient series T_1 and T_2, we submitted them into the following equation to reconstruct the forecast SSTA field:

$$\hat{x}_t = \sum_{n=1}^{2} E_n \bullet T_{nt}, t = 1,2,...,12 \qquad (8)$$

where E_n , T_{nt} are the EOF space fields and forecast time coefficients, respectively, and $\hat{x}_{tj}$ is the forecast SSTA field reconstructed by EOF.

After reconstruction of the space mode (treated as constant) and time coefficient series (model prediction), the forecast of the SSTA fields was obtained, based on the forecast results of T_1 and T_2 in Section 5.2. For economy of space, we cannot draw all of the forecasted SSTA fields, so we selected a strong El Niño event (December 1997), a strong La Niña event (December 1999) and a neutral event (November 2002) as examples.

Fig. 6 shows the forecast SSTA field during a strong El Niño event. From the actual SSTA field in December 1997 (Fig. 6a), an obvious warm tongue structure occurred in the area of [10 °S～5 °N，90 °W～150 °W] in the Eastern Equatorial Pacific, and a warm anomalous distribution arose in the west Pacific, which indicated a weak El Niño event. The forecasted SSTA field of December 1997 is shown in Fig. 6b. Although the range of warm tongue was a litter bigger than the actual situation, the forecast shape was similar to the actual field and also the contour lines were similar. The average MAPE between the forecast field and the actual field is 8.56%, which was controlled within 10%. The forecast results of the improved model event were quite good for the El Niño event.

Fig.7 shows the forecasted SSTA field of a strong La Niña event. From the actual SSTA field in December 1999 (Fig. 7a), an obvious cold pool occurred in the area of [10 °S～10 °N，120 °W～180 °W] in the Equatorial Pacific, which covered the Niño3.4

area. This SSTA field presented a strong strength La Niña event. The forecast SSTA field from December 1999 is shown as Fig. 7b. Although the strength of the cold pool was weaker than the actual situation, the forecast shape was similar to that of the actual field. The average MAPE between the forecast field and the actual field was 9.69%. The errors were larger than that of the El Niño event, but they can be controlled within 10%, which is acceptable.

Fig. 8 shows the forecasted SSTA field of a neutral event. From the actual SSTA field in November 2002 (Fig. 8a), a warm pool occurred in the area of [10 °S～10 °N，120 °W～180 °W] in the Equatorial Pacific, which covered the Niño3.4 area. However, the warm pool was small and weak, which represented a neutral event. The forecasted SSTA field from November 2002 is shown in Fig. 8b. Comparing Figures 6, 7 and 8, we can see that the forecasted SSTA field of a neutral event was a little worse than that of the El Niño and La Niña events. The forecasted shape of the SSTA field basically described the actual situation, but the warm pool in the Niño3.4 area was stronger and bigger than that of the actual situation, which indicated a borderline El Niño event. The average MAPE between the forecasted field and the actual field was 14.50%, which was big but can be accepted.

We obtained the average values of MAPE of 18 El Niño events, 22 La Niña events and 20 neutral events, which were 9.52%, 9.88% and 14.67%, respectively, representing a good SSTA field forecasting ability of our model.

5.4 Forecast of ENSO index

The ENSO index can be represented as the sea surface temperature anomaly

(SSTA) in the Niño-3.4 region (5 °N-5 °S, 120 °-170 °W) and the ENSO index forecast was the 3-month forecast (Barnston et al. 2012). So we also can pick up the ENSO index from the above forecasted SSTA field. The forecast results of the ENSO index within 20 months can also be obtained. The definition of lead time can be seen in the reference (Barnston et al. 2012). Therefore, similar to the forecast experiment in section 5.1, a succession of running 3-month mean SST anomalies with respect to the climatological means for the respective prediction periods, averaged over the Niño 3.4 region, can be obtained, as demonstrated in Fig. 9.

The evaluation criteria of the ENSO index is the temporal correlation (TC), its definition and specific calculation steps can be seen in these literatures (Kathrin et al.,2016; Nicosia et al. 2013); The TC is often used to measure the prediction effect of the ENSO index. For example, Barnston et al.in 2012 also used the TC to compare the forecast skill of 21 real-time seasonal ENSO models.

The forecast results within lead times of 18 months are shown in Fig. 9, which demonstrate that the forecast results of the ENSO index are good. Within lead time of 12 months, the TC was 0.8985 and the MAPE value was small, only 8.91%. In addition, the borderline La Niña event in 2008–2009 was predicted well. After lead times of 12 months, forecasts began to diverge and the errors started to increase. Although the TC remained approximately 0.61, MAPE reached 18.58%. Therefore, a moderate strength El Niño event that occurred in 2009/10 was not predicted.

We should give more examples to test the ENSO prediction ability of our model. As in section 5.3, we can divide 60 examples as three types, which are examples of

ElNiño year, LaNiña year and neutral year. Finally, we can obtain the forecast results of different types of examples in different lead times, as shown in table 4.

From table 4, the average TC of 60 experiments was 0.712 and the average MAPE was 7.62% within 12 months for all seasons of lead time, which indicates that the overall ENSO forecast ability of our model was good. The forecast results of the El Niño examples were significantly worse than those of La Niña examples, while the forecast results of La Niña examples were significantly worse than those of neutral examples, which show the model forecast ability of the abnormal state was worse than the normal state of the ENSO index. Even for the forecast results of El Niño examples, the average TC was still above 0.6 and the average MAPE can be controlled below 10%, which means the forecast results were still in the acceptable range. Our model not only accurately predicted the stronger El Niño and La Niña phases but also the neutral states.

The ENSO forecast often had a spring predictability barrier (Webster, 1999), which was most prominent during decades of relatively poor predictability (Balmaseda et al., 1995).To test our model, the skill should be computed over the entire time series and separately for seasonal subsets of the time series. From the table4, we can see that although the forecast results of the present model in the spring were worse than in the autumn, the margin was not high, which means the model can overcome the "spring predictability barrier," to some extent.

5.5 Compared with six mature models

Barnston et al. (2012) compared many ENSO forecast models. Based on his

533 research, we selected four high quality dynamical models, including ECMWF, JMA,
534 the National Aeronautics and Space Administration Global Modelling and
535 Assimilation Office (NASAGMAO) and the National Centre for Environmental
536 Prediction Climate Forecast System (NCEP CFS; Version1). Two high quality
537 statistical models also be selected, including the University of California, Los Angeles
538 Theoretical Climate Dynamics (UCLA-TCD) multilevel regression model and the
539 NOAA/NCEP/CPC constructed Analogue (CA) model. The detail of the above
540 models can be seen in these references (Reynolds al., 2002; Luo et al., 2005; Barnston
541 et al., 2012).

542 We then compared the forecast ability of the above six models with that of our
543 model. All of the experiments of our model and six other models were conducted
544 under the same conditions using the same historical data for modelling and the same
545 initial values to forecast. In the CPC website, there are detailed explanations of six
546 models' training samples and the initial values. So we do not need to install all these
547 models on their own machines and run them for forecasting. We just made training
548 samples and initial values of our model were the same with those of selected six
549 models. At an 8-month lead time, the TC of our model for all seasons combined was
550 0.613 (Fig. 10). In brief, the forecast ability of the ECMWF model was slightly better
551 than that of our model but the ability of the other 5 models was worse than that of our
552 model. While, in regard to the forecast length, the TC within 12 months of our model
553 is greater than 0.6, which was superior to the ECMWF model. In addition, the forecast
554 results of the UCLA-TCD model and the CPC CA model reduced quickly after

555 5-month lead times, so the forecast ability of our model was more stable than them.

556 The root mean square error (RMSE) was also examined to assess the
557 performance of discrimination and calibration. Barnston et al. (2012) believed that all
558 seasonal RMSE values contributed equally to a seasonally combined RMSE. So we
559 drew figure 11 to show seasonally combined RMSE.

560 From Fig. 10 and Fig. 11, we can see the highest correlation tend to have
561 lower RMSE. So the RMSE of our model was slightly higher than that of ECMWF
562 model, but it was much lower than those of the other 5 models. Figure 11 and Figure
563 12 is the average TC and RMSE of the 240 experiments of compared with six mature
564 models, covers a variety of different types of ENSO and different lead time. So those
565 samples should be really representative.

566 6. Conclusions and discussion

567 6.1 Conclusions

568 A new forecasting model of the SSTA field was proposed based on a dynamical
569 system reconstruction idea and the principle of self-memorization. The approach of
570 the present paper consisted of the following steps:

571 (1) The SST field can be time (coefficients)-space (structure) deconstructed
572 using the EOF method. Take T_1, T_2, SOI and EAWMI and consider them as
573 trajectories of a set of four coupled quadratic differential equations based on the
574 dynamical system reconstruction idea. The parameters of this dynamical model were
575 estimated using a GA.

576 (2) The forecast results of the dynamical model can be improved by the

self-memorization principle. The memory coefficients in the improved self-memorization model were obtained using the GA method.

(3) The long-term step-by-step forecast results and cross-validated retroactive hindcast results of time series T_1 and T_2 are all found to be good, with the CC of approximately 0.80 and the MAPE of less than 15%.

(4) The improved model was used to forecast the SSTA field. The forecasted SSTA fields of three types of events are accurate. Not only is the forecast shape similar to the actual field but also the contour lines are similar.

(5) The improved model was also used to forecast the ENSO index. The average TC of 60 examples within 12 months is 0.712, and the MAPE value is small, only 7.62%, which proves that the improved model has better forecasting results of the ENSO index. Although the forecast results of the model in the summer were worse than in the winter, the margin was not high, which means that the model can overcome the spring predictability barrier to some extent. Finally, compared with the six mature models, the new dynamical-statistical forecasting model has a scientific significance and practical value for the SST in the eastern equatorial Pacific and El Niño/La Niña event predictions.

6.2 Discussion

L'Heureux et al.(2013) reported that using different data sets and time periods, the 2nd EOF is not stable, being entirely due to the strong trend. So we need to do more experiments to prove that we choose the second mode of EOF to be appropriate, and whether different time periods will make us forecast unstable or not. Our original

599 data is the monthly average SST data from January 1951 to Dec. 2010, which are 60
600 years. We will increase the length of the data for 20 years (Jan.1931 –Dec.2010), for
601 10 years (Jan.1941- Dec.2010) and decrease the length of the data for 10 years
602 (Jan.1961- Dec.2010), for 20 years (Jan.1971- Dec.2010). And then we use the same
603 method to reconstruct a model and forecast the ENSO index as section5.4.The results
604 show in the 60 experiments, the difference among forecast results of both TC and
605 MAPE of five different sample data are less, and no abnormal change suddenly worse
606 or better appear. All these indicate that using different data sets and time periods, even
607 though may have a certain impact on the pattern of the 2nd EOF, but the impact on
608 our forecast is not great and it will not make our forecast unstable.

609 Actually, how many variables and which variables are used in our model
610 become a key issue to be resolved. We are a complex four factor differential
611 equations coupling model. We are a complex coupled model of four factor differential
612 equations, so we are more concerned with the correlation between each other. The
613 correlation must be considered as an important criterion to select the factors, but in
614 order to further verify the correctness of the selection criterion, we have carried out
615 the prediction experiments (the 60 cross-validated retroactive hindcasts experiments
616 of the ENSO index for all seasons combined at lead times of 8 months) of different
617 variables.

618 We can see that for all the forecast results of the models of different variables,
619 the prediction results of T_1, T_2, SOI is the best among those of the three factors and the
620 prediction result of $T_1, T_2, \mathrm{SOI}, \mathrm{EAWMI}$ is the best among those of the four factors. But

621 the prediction result of $T_1,T_2,\mathrm{SOI},\mathrm{EAWMI}$ is best among all, which proves that our
622 selection factors are correct. In our previous study (Hong et al., 2015), the model of
623 the Western Pacific subtropical high was established by using the correlations as a
624 criterion to select factors and their forecast results are also good. Now we use the
625 correlations as a criterion to select factors is also in line with our previous research.
626 Based on the definition of overfitting and the previous studies(Golbraikh et al.,
627 2003; Everitt and Skrondal,2010), there is no evidence that more parameters will be
628 certain to result in overfitting. We can judge whether a model is overfitting or not by
629 the accuracy of prediction results of independent samples (Golbraikh and Tropsha,
630 2002; Qin and Li, 2006).
631 In the sample training, our model does not purposely pursue the high degree of
632 the training samples fitting and improve the effectiveness of the independent
633 generalization. In fact in our paper the forecast results of the cross-validated
634 retroactive hindcasts (section 5.2) and the independent samples validation (table3 and
635 table4) are both good. Especially, the independent samples validation of the ENSO
636 index as the table4, we have carried out the 240 independent sample validation
637 prediction of four seasons of different ENSO events and the coverage of independent
638 samples test is very wide. Moreover, compared with 6 mature prediction models, the
639 forecast results of our model are also good, which prove the overfitting problem does
640 not exist in our model. So according to the definition of overfitting, we can say the
641 over fitting phenomenon does not exist in our model.
642 Compared with the original model, why the improved model has good forecast

643 results and can overcome the spring predictability barrier to some extent are as follow:
644 Recently, many studies have pointed out that spring is the most unstable season of the
645 air - sea interaction and the error is likely to develop or grow in the spring, resulting in
646 the spring predictability barrier (Zhang et al, 2012; Philander et al., 1992). When the
647 original model uses the indexes in summer as the initial values to predict, the SOI
648 factor representing the air-sea interaction is most unstable in the spring and the
649 EMWMI factor does not have much influence on ENSO in summer, so the forecast
650 results using the indexes in summer as the initial values are certainly much worse than
651 those using the indexes in the winter as the initial values. That is why our original
652 model does not overcome the spring predictability barrier.

653 However, the introduction of the self-memorization dynamics principle can help
654 our model overcome the spring predictability barrier to some extent. Although the
655 lead time is still summer (such as JJA), the information of the initial value actually
656 contains the previous p + 1 month (in this case p = 6, which contains the information
657 of the previous seven months, including the information of T_1, T_2 , SOI, EMWMI
658 factor in winter (January, February), spring (March, April, May) and summer (June
659 and July)). From the dynamical analysis, in this situation, the information and
660 interaction relationship of four factors have been a long period (from winter to
661 summer) accumulated, containing much air-sea interaction processes and winter
662 monsoon continued abnormal information, so the forecast results of our improved
663 model will be much better than the original model which simply uses only one initial
664 value. That is why the improved model overcomes the spring predictability barrier to

some extent.

The forecast results of our model are good, but it still has some problems:

(1) The inclusion of these terms and the physical processes do these terms in equation (2) represent are important, especially for the discussion of dynamical characteristics of the dynamical model. But now we are difficult to give a clear meaning. Now the main work of our paper is the prediction experiments of the model. For the reason of time and length, this paper mainly discusses the prediction results of the model. The physical processes do these terms represent and the discussion of the dynamical characteristics of the model will be the focus of our next work. Before this, we have also used the Takens' delay embedding theorem to reconstruct the dynamical model of the Western Pacific subtropical high(WPSH). And Based on the reconstructed dynamical model, dynamical characteristics of WPSH are analyzed and an aberrance mechanism is developed, in which the external forcings resulting in the WPSH anomalies are explored, which have been published (Hong et al., 2016). We also study the bifurcation and catastrophe of the West Pacific subtropical high ridge index of a nonlinear model (Hong et al., 2017). Based on our previous method and work, our next work is to analyse the physical processes and the dynamical characteristics of the SST field.

(2)The experiments in the present study have proven that the forecasting results of the improved model are good for large-scale systems, such as ENSO events, and the forecasting period has been extended. However, for small-scale systems, such as Hurricanes, whether the forecast results could be improved using the present

687 improved model needs to be further verified.

688 (3) Our paper focuses primarily on these defined indices with T_1, T_2 to
689 reconstruct a prediction model. Maybe, we can select variables (predictor) based on
690 EOF analysis and our model may be a more physically oriented model. Maybe we can
691 learn from Yim et al. (2013; 2015) to draw correlation maps between these fields and
692 the SSTA field and select the predictors from physical considerations. All these above
693 questions require that a lot of experiments to be carried out.

694 These items will be our future work.

695

696 **Acknowledgments** This study was supported by the Chinese National Natural
697 Science Fund (no. BK20161464) of Jiangsu Province and the Chinese National
698 Natural Science Fund (nos. 41375002，41075045, 41306010, 41571017, 51190091
699 and 41071018) , the Program for New Century Excellent Talents in University
700 (NCET-12-0262), the China Doctoral Program of Higher Education
701 (20120091110026), the Qing Lan Project, the Skeleton Young Teachers Program, and
702 the Excellent Disciplines Leaders in Midlife-Youth Program of Nanjing University.

703

704 **APPENDIX A: THE PRINCIPLE OF DYNAMICAL MODEL**
705 **RECONSTRUCTION**

706 Suppose that the physical law of a nonlinear system going by over time can be
707 expressed as the following difference form:

708 $$\frac{q_i^{(j+1)\Delta t} - q_i^{(j-1)\Delta t}}{2\Delta t} = f_i(q_1^{j\Delta t}, q_2^{j\Delta t}, ..., q_i^{j\Delta t}, ..., q_N^{j\Delta t}) \quad j = 2,3,.....M-1 \qquad \text{(A1)}$$

where f_i is the generalized nonlinear function of $q_1, q_2, \ldots q_i, \ldots q_N$, N is the number of variables, and M is the length of observed data. $f_i(q_1^{j\Delta t}, q_2^{j\Delta t}, \ldots, q_i^{j\Delta t}, \ldots, q_N^{j\Delta t})$ can be assumed to contain two parts: G_{jk} representing the expanding items which contain variable q_i, P_{ik} just representing the corresponding parameters which are real numbers ($i = 1, 2, \ldots N$, $j = 1, 2, \ldots M$, $k = 1, 2, \ldots, K$).

It can be supposed as follows:

$$f_i(q_1, q_2, \ldots, q_n) = \sum_{k=1}^{K} G_{jk} P_{ik} \tag{A2}$$

$D = GP$ is the matrix form of Eq.(A2) , in which

$$D = \begin{Bmatrix} d_1 \\ d_2 \\ \cdots \\ d_M \end{Bmatrix} = \begin{Bmatrix} \frac{q_i^{3\Delta t} - q_i^{\Delta t}}{2\Delta t} \\ \frac{q_i^{4\Delta t} - q_i^{2\Delta t}}{2\Delta t} \\ \cdots \\ \frac{q_i^{M\Delta t} - q_i^{(M-2)\Delta t}}{2\Delta t} \end{Bmatrix}, \quad G = \begin{Bmatrix} G_{11}, G_{12}, \ldots\ldots G_{1K} \\ G_{21}, G_{22}, \ldots\ldots G_{2,K} \\ \cdots \\ G_{M1}, G_{M2}, \ldots\ldots G_{M,K} \end{Bmatrix}, \quad P = \begin{Bmatrix} P_{i1} \\ P_{i2} \\ \cdots \\ P_{iK} \end{Bmatrix} \tag{A3}$$

Parameters of the above equation can be determined through inverting the observed data. Vector P which satisfies the above equation can be solved, based on a given vector D. Assuming q is unknown, it is a nonlinear system. However, assuming P is unknown, it is a linear system.

With the restriction $S = (D - GP)^T (D - GP)$ as a minimum, GA is introduced as an optimization solution search in the model parameters space.

Assuming that the parameters matrix P is the population (solutions), the $S = (D - GP)^T (D - GP)$ is an objective function, $l_i = \frac{1}{S}$ is the value of individual fitness, and $L = \sum_{i=1}^{n} l_i$ is the value of total fitness. The operating steps of GA include: creation and coding of initial population (solutions), fitness calculation, the choice of male parents, crossover and variation, etc. A detailed theoretical explanation can be

729 got from Wang (2001). The step length is 1 month during the calculation. After
730 optimization searches and genetic operations, the target value can be rapidly
731 converged on and each optimal parameter of the dynamical equations can be obtained.
732 Through the above approach, we can obtain parameters of a nonlinear
733 dynamical system, and reconstruct the nonlinear dynamical equations from observed
734 data.
735
736 **APPENDIX B: THE MATHEMATICAL PRINCIPLE OF**
737 **SELF-MEMORIZATION DYNAMICS OF SYSTEMS**
738 The dynamical equations of a system can be expressed as:
739 $$\frac{\partial x_i}{\partial t} = F_i(x, \lambda, t) \; i = 1, 2, ..., J \qquad \text{(B1)}$$
740 where J is an integer， x_i is the *i*th variable of the system state, and λ is
741 the parameter. Equation (B1) represents the relationship between a source function
742 F and a local change of x . Obviously, x is a scalar function with time t and
743 space r_0 . A set of time $T = [t_{-p} ... t_0 ... t_q]$ can be considered, where t_0 is an initial
744 time. A set of space $R = [r_a ... r_i ... r_\beta]$ can be considered, where r_i is a spatial point.
745 An inner product in space $L^2 : T \times R$ is defined by:
746 $$(f, g) = \int_a^b f(\xi) g(\xi) d\xi, \; f, g \in L^2 \qquad \text{(B2)}$$
747 Accordingly, a norm can be defined as:
748 $$\| f \| = [\int_a^b (f(\xi)^2 d\xi]^{1/2}$$

For a completion L^2, it can become a Hilbert space H. A generalized one in H can be regarded as a solution of the multi-time model. By introducing a memorization function $\beta(r,t)$, we can obtain:

$$\int_{t_0}^{t} \beta(\tau)\frac{\partial x}{\partial \tau}d\tau = \int_{t_0}^{t} \beta(\tau)F(x,\tau)d\tau \qquad \text{(B3)}$$

where r in $\beta(r,t)$ can be dropped through fixing on the spatial point r_0. Suppose that function $\beta(r,t)$ and variable x etc. are all continuous, differentiable and integrable, an integration by the left parts of Eq. (B3) can be made as:

$$\int_{t_0}^{t} \beta(\tau)\frac{\partial x}{\partial \tau}d\tau = \beta(t)x(t) - \beta(t_0)x(t_0) - \int_{t_0}^{t} x(\tau)\beta'(\tau)d\tau \qquad \text{(B4)}$$

where $\beta'(t) = \partial\beta(t)/\partial t$. The mean value theorem can be introduced into the third term in Eq. (B4), the following equation can be obtained:

$$-\int_{t_0}^{t} x(\tau)\beta'(\tau)d\tau = -x^m(t_0)[\beta(t) - \beta(t_0)] \qquad \text{(B5)}$$

where $x^m(t_0) \equiv x(t_m), t_0 < t_m < t$. Substituting Eq. (B4) and Eq. (B5) in Eq. (B3) and carrying out an algebraic operation, the following equation can be obtained:

$$x(t) = \frac{\beta(t_0)}{\beta(t)}x(t_0) + \frac{\beta(t) - \beta(t_0)}{\beta(t)}x^m(t_0) + \frac{1}{\beta(t)}\int_{t_0}^{t} \beta(\tau)F(x,\tau)d\tau \qquad \text{(B6)}$$

Because the x value which is at initial time t_0 and middle time t_m, only on the fixed point r_0 itself , relates to the first term and the second term in Eq. (B6) , they are be called as a self-memory term. Also, we can call the third term as an exogenous effect, i.e., which is contributed by other spatial points.

Similarly as Eq. (B4), for multi-time t_i, $i = -p, -p+1..., t_0, t$, it gives

$$\int_{t_{-p}}^{t_{-p+1}} \beta(\tau)\frac{\partial x}{\partial \tau}d\tau + \int_{t_{-p+1}}^{t_{-p+2}} \beta(\tau)\frac{\partial x}{\partial \tau}d\tau + ... + \int_{t_0}^{t} \beta(\tau)\frac{\partial x}{\partial \tau}d\tau = \int_{t_{-p}}^{t} \beta(\tau)F(x,\tau)d\tau .$$

After the same term $\beta(t_i)x(t_i), i = -p+1, -p+2, ..., 0$ was eliminated, we have

$$\beta(t)x(t) - \beta(t_{-p})x(t_{-p}) - \sum_{i=-p}^{0}[\beta(t_{i+1}) - \beta(t_i)]x^m(t_i) - \int_{t_{-p}}^{t} \beta(\tau)F(x,\tau)d\tau = 0 \quad \text{(B7)}$$

As a matter of convenience, we set $\beta_t \equiv \beta(t), \beta_0 \equiv \beta(t_0), x_t \equiv x(t), x_0 \equiv x(t_0)$; the following text uses similar notations. Then, Eq. (B7) can be expressed as:

$$\beta_t x_t - \beta_{-p} x_{-p} - \sum_{i=-p}^{0} x_i^m(\beta_{i+1} - \beta_i) - \int_{t_{-p}}^{t} \beta(\tau)F(x,\tau)d\tau = 0 \quad \text{(B8)}$$

Setting $x_{-p} \equiv x_{-p-1}^m, \beta_{-p-1} = 0$, the Eq. (B8) can be written as:

$$x_t = \frac{1}{\beta_t}\sum_{i=-p-1}^{0} x_i^m(\beta_{i+1} - \beta_i) + \frac{1}{\beta_t}\int_{t_{-p}}^{t} \beta(\tau)F(x,\tau)d\tau = S_1 + S_2 \quad \text{(B9)}$$

S_1 is called as a self-memory term and S_2 is called as an exogenous effect term.

For the convenience of calculations, the above self-memorization equation can be discretized. The differential by difference and the summation can replace the integration in Eq. (B9), and the mean of two values which are at adjoining times; i.e., $x_i^m \approx \frac{1}{2}(x_{i+1} + x_i) \equiv y_i$ can simply replace x_i^m.

Taking an equal time interval $\Delta t_i = t_{i+1} - t_i = 1$ and incorporating β_i and β_t, we can obtain a discretized self-memorization equation as follows:

$$x_t = \sum_{i=-p-1}^{-1} \alpha_i y_i + \sum_{i=-p}^{0} \theta_i F(x,i) \quad \text{(B10)}$$

where F is the dynamical kernel of the self-memorization equation, $\alpha_i = \frac{(\beta_{i+1} - \beta_i)}{\beta_t}$; $\theta_i = \frac{\beta_i}{\beta_t}$.

Based on Eq. (B10), the above technique performed computations and the forecast can be called as a self-memorization principle.

REFERENCES

Ashok K, Guan Z, Yam agata T : Impact of the Indian Ocean Dipole on the decadal relationship between the Indian mon soon rainfall and ENSO, Geophys Res Let,28(23), 4499-4502, 2001.

Balmaseda M.A., Davey M.K. and Anderson D.L.T.: Decadal and seasonal dependence of ENSO prediction skill,J Clim.,8, 2705–2715, 1995.

Barnston A. G., et al.: Skill of real-time seasonal ENSO model predictions during 2002-2011,Bull. Amer. Meteor. Soc.,93, 631-651, 2012.

Belkin M. and P. Niyogi: Laplacian eigenmaps for dimensionality reduction and data representation,Netural Comput.,15,1373-1391, 2003.

Bjerknes J.: Atmsopheric telconnections from the equtorail Pacific,Mon. Wea. Rev.,97,163-172, 1969.

Cao H. X.: Self-memorization Equation in Atmospheric Motion,Science in China (Series B),36(7), 845-855, 1993.

Chen D., S. E. Zebiak, A. J. Busalacchi and M. A. Cane: An Improved Procedure for El Nirio Forecasting: Implications for Predictability,Science, 269, 1699-1702, 1995.

Chen G., Shao B. M. Han Y., et al.: Modality of semiannual to multidecadal oscillations in global sea surface temperature variability. Journal of Geophysical Research, 115, 1-14, 2010.

Chen X. D., Xia J., Xu Q.: Differential Hydrological Grey Model(DHGM) with self-memory function and its application to flood forecasting,Sci China Tech Sci.,52,1039–1049, 2009.

Clarke A. J. and S. Van Gorder: Improving El Niño prediction using a space-time integration of Indo-Pacific winds and equatorial Pacific upper ocean heat content, Geophys. Res. Lett.,30,1399. doi:10.1029/2002GL016673, 2003.

Delecluse P., Davey M., Kitamura Y., Philander S., Suarez M., Bengtsson L.: TOGA review paper: coupled general circulation modeling of the tropical Pacific,J Geophys Res,103,14357–14373, 1998.

Davey M., Huddleston M., Sperber K.R., et al.: A study of coupled model climatology and variability in tropical ocean regions,Clim. Dyn.,18,403–420, 2002.

816 Dommenget and Latif: A Cautionary Note on the Interpretation of EOFs, Journal of
817 Climate,15(2),216–225, 2002.
818 Drosdowsky W.: Statistical prediction of ENSO (Niño 3) using sub-surface temperature data,Geophys.
819 Res.Lett., 33 , L03710. doi:10.1029/2005GL024866, 2006.
820 Everitt B.S., Skrondal A.: Cambridge Dictionary of Statistics, Cambridge University Press, 2010.
821 Feng G. L., Cao H. X., Gao X. Q., et al.: Prediction of precipitation during summer monsoon with
822 self-memorial model,Adv Atmos Sci.,18 ,701–709, 2001.
823 Fraedrich K.: Estimating weather and climate predictability on attractors,J .A tmos.Sci.,44,7 22-728,
824 1987.
825 Glantz MH, Katz RW, Nicholls N (eds): Teleconnections linking worldwide climate anomalies,
826 74pp,Cambridge University Press, Cambrige, UK, 1991.
827 Golbraikh A. and Tropsha A.: Beware of q 2 ! Journal of Molecular Graphics and Modelling, 20 ,
828 269–276, 2002.
829 Golbraikh A.,Shen M., Xiao Z. Y., Xiao Y. D., Lee Kuo-Hsiung, Tropsha A.: Rational selection of
830 training and test sets for the development of validated QSAR models. Journal of Computer-Aided
831 Molecular Design, 17(2), 241-253, 2003.
832 Gu X. Q.: A spectral model based on atmospheric self_memorization principle,Chinese Science
833 Bulletin,43(20),1692-1702 , 1998.
834 Hong M., Zhang R., Wu G. X., et al.,: A Nonlinear Dynamic System Reconstruction of the Subtropical
835 High Characteristic Index based on Genetic Algorithm. Chinese Journal of Atmospheric
836 Sciences,31(2):346-352, 2007.
837 Hong M., Zhang R.andMa C. C.et al.: A Non-Linear Dynamical–Statistical Model for Reconstruction
838 of the Air–Sea Element Fields in the Tropical Pacific Ocean,Atmosphere-Ocean, doi:
839 10.1080/07055900.2014.908765, 2014.
840 Hong M., Zhang R., et al.: Reconstruction and forecast experiments of a statistical-dynamical model of
841 the Western Pacific subtropical high and Eastern Asian summer monsoon factors，Weather and
842 Forecasting, 30:206-216 , 2015
843 Hong M., Zhang R., et al.: Catastrophe and Mechanism Analyses of Multiple Equilibria in the Western
844 Pacific Subtropical High System Based on Objective Fitting of Spatial Basis Functions. Monthly
845 Weather Review, 144, 997-1015, 2016.

Hong M., Zhang R., et al.: Bifurcations and catastrophes in a nonlinear dynamical model of the western Pacific subtropical high ridge line index and its evolution mechanism, Theor. Appl. Climatol., 129, 363-384, 2017.

Hu, T.S., K.C. Lam, and S.T. Ng: River flow time series prediction with a range-dependent neural network,Hydrol. Sci. J., 46, 729–745, 2001.

Hu Y. J., Zhong Z., Zhu Y. M. et al.: A statistical forecast model using the time-scale decomposition technique to predict rainfall during flood period over the middle and lower reaches of the Yangtze River Valley. Theoretical and Applied Climatology, doi: 10.1007/s00704-017-2094-9,2017.

Huang. J., Y. Yi, S. Wang, et al.: An analogue-dynamical long-range numerical weather prediction system incorporating historical evolution,Quart J Roy Meteor Soc, 119(511),547-565, 1993.

Islam M.N. Sivakumar B.: Characterization and prediction of runoff dynamics:a nonlinear dynamical view. Advances in Water Resources, 25, 179-190, 2002.

James A. Carton and Benjamin S. Giese: A Reanalysis of Ocean Climate Using Simple Ocean Data Assimilation (SODA),Monthly Weather Review,136(8),2999-3011 , 2008.

Jin E. K.，James L. K.，Wang B.，et a1.: Current status of ENSO prediction skill in coupled ocean-atmosphere models,Climate Dyn,31, 647-664, 2008.

Johnson S.D., Battisit D.S. andSarachik E. S.: Empirically Derived Markov Models and Prediction of Tropical Pacific Sea SurfaceTemperature Anomalies, Journal of Climate,13,3-17, 2000.

Kalnay E., Kanamitsu M. and Kistler R.: The NCEP/NCAR 40-year reanalysisproject, Bull. Amer. Meteor. Soc.,77,437-470 , 1996.

Kathrin Büttner, Jennifer Salau, and Joachim Krieter: Temporal correlation coefficient for directed networks. Springerplus, 5(1): 1198-1203, 2016.

Kim Ji-Won ,Soon-Il An,Sang-Yoon Jun,Hey-Jin Park,Sang-Wook Yeh.: ENSO and East Asian winter monsoon relationship modulation associated with the anomalous northwest Pacific anticyclone, Climate Dynamics, 49(4), 1157–1179, 2017.

L'Heureux Michelle L., Collins Dan C., Hu Zeng-Zhen. Linear trends in sea surface temperature of the tropical Pacific Ocean and implications for the El Nin˜o-Southern Oscillation, Climate Dynamics, 40, 1223–1236, 2013.

Liebmann B. and C.A. Smith: Description of a Complete (Interpolated) Outgoing Longwave Radiation Dataset,Bulletin of the American Meteorological Society,77,1275-1277, 1996.

Luo, J.-J., S. Masson, S. Behera, S. Shingu, andT. Yamagata: Seasonal climate predictabilityin a

877 coupled OAGCM using a different approach forensemble forecasts,J. Climate, 18,4474–4497, 2005.
878 Mechoso C.R., Robertson A.W., Barth N., et al.: The seasonal cycle over the tropical Pacific in coupled
879 atmosphere–ocean generalcirculation models,Mon Weather Rev,123,2825–2838, 1995.
880 Molteni F., et al.: ECMWF seasonal forecast system3,CLIVAR Exch,43,7-9, 2007.
881 Moore A. M., Zavala-Garay J. and Tang Y., et al.: Optimal forcing patterns for coupled models of
882 ENSO,J Climate,19,4683-4699 , 2006.
883 Neelin J.D., Latif M. and Allaart M.A.F.: Tropical air-sea interaction in general circulation
884 models,Clim Dyn.,7,73–104, 1992.
885 Nicosia V, Tang J, Mascolo C, Musolesi M, Russo G, Latora V: Graph metrics for temporal networks.
886 In: Holme P, Saramäki J, editors. Temporal networks. Berlin: Springer, pp. 15–40, 2013,.
887 Palmer T. N., Alessandri A. and Andersen U., et al.: Development of a European multi-model
888 ensemble system forseasonal to interannual prediction (DEMETER),Bull Amer Met Soc.,85,853-872 ,
889 2004.
890 Philander S G., Pacanowski R.C., N-C Lau et al.: Simulation of ENSO with a global atmospheric GCM
891 coupled to a high resolution, tropical Pacific Ocean GCM. *J.Climate, 5*,308-329,1992.
892 Qin G. H. and Li Z. H.: Over-fitting of BP NN research and its application, Engineering Journal of
893 Wuhan University,39(6),1671-1679 , 2006.
894 Rasmusson E.M. and Carpenter T.H.: Variations in tropical seasurface temperature and surface wind
895 fields associated with the Southern Oscillation/E1 Niño,Mon Weather Rev.,10, 354-384, 1982.
896 Rayner NA, Parker DE, Horton EB, Folland CK, Alexander LV, Rowell DP, Kent EC, Kaplan A:
897 Global analyses of sea surface temperature, sea ice, and night marine air temperature since the late
898 nineteenth century. J Geophys Res 108(D14):4407. doi:10.1029/2002JD002670, 2003.
899 Reynolds, R. W., N. A. Rayner, T. M. Smith, D. C.Stokes, and W. Wang: An improved in situand
900 satellite SST analysis for climate,J. Climate,15,1609–1625, 2002.
901 Saha S., Nadiga C. and Thiaw J., et al.: The NCEP climate forecast system,Journal of
902 Climate,19 ,3483-3517 , 2006.
903 Saji N. H., Goswami B. N., V. inayachandran P. N., et al.: A dipole mode in the tropical Indian
904 Ocean,Nature, 401(6751),360-363, 1999.
905 Smith T.M.: Improved extended reconstruction of SST(1854-1997). J. Climate, 17, 2466-2477, 2004.

Takens, F.: Detecting strange attractors in fluid turbulence,Lecture Notes in Mathematics,898(2),361-381 , 1981.

Sivakumar B, Berndtsson R, Persson M.: Monthly Runoff Prediction Using Phase -space Reconstruction. Hydrological Sciences Journal, 46(3), 377 -388, 2001.

Sivakumar B., Jayawardena A.W., Fernando T.M.K.G.,: River flow forecasting: use of phase-space reconstruction and artificial neural networks approaches. Journal of Hydrology, 265, 225-245, 2002.

Timmermann A., Voss H. U. and Pasmanter R.: Empirical Dynamical System Modeling of ENSO Using Nonlinear Inverse Techniques, Journal of Physical Oceanography, 31,1579-1598 , 2001.

Tomita, T., and T. Yasunari: Role of the northeast winter monsoon on the biennial oscillation of the ENSO/monsoon system,J. Meteor. Soc. Japan, 74,399–413 , 1996.

Trenberth, E. K., et al.: Progress during TOGA in understanding and modeling global teleconnections associated with tropical sea surface temperatures,J. Geophys. Res., 107, C7, 14291-14324,1998.

Wang B., Wu R., Lukas R.: Roles of western North Pacific wind variation in thermocline adjustment and ENSO phase transition,J Meteor Soc Japan,77,1-16,1999a.

Wang B., Wu R., Li T.: Atmoshere-warm ocean interaction and its impacts on Asian-Australian monsoon variation. J. Climate, 16, 1195-1211, 2003.

Wang B.，Lee J. Y.，Shukla J.，et al.: Advance and prospectus of seasonal prediction：assessment of the APCC／CIiPAS 14-Model Ensemble Retrospective Seasonal Prediction(1980—2004),Climate Dyn.,33(1),93-117 , 2009a.

Wang C., Weisberg R. H. and Virmani J. I.: Western Pacific interannual variability associated with the El Niño-Southern Oscillation,J Geophy Res.,104,5131-5149, 1999b.

Wang, L., W. Chen, and R. H. Huang: Interdecadal modulation of PDO on the impact of ENSO on the east Asian winter monsoon, Geophys. Res. Lett., 35, L20702, doi:10.1029/2008GL035287, 2008.

Wang, W. C., K. W. Chau, C. T. Cheng, and L. Qiu: A comparison of performance of several artificial intelligence methods for forecasting monthly discharge time series. J. Hydrol., 374, 294–306, doi:10.1016/j.jhydrol.2009.06.019,2009b.

Wang L.: Intelligent Optimization Algorithms and Its Application, pp. 23-24, Tsinghua University Press, Chendu, 2001.

Webster P. J., Moore A. M., Loschnigg J. P., et al.: Coupled ocean-atmosphere dynamics in the Indian Ocean during 1997- 98, Nature, 401(6751),356-360, 1999.

936 Weinberger K. Q. and L. Saul: Unsupervised learning of image manifolds by semidefinite
937 programming,Int. J. Comput. Vision.,70, 77-90, 2006.
938 Xu B.C., Wang Z.S., Wu J.P. and Zhou E.M.: Interaction between sea surface temperature (SST) of
939 information regions and southern oscillation index (SOI) in Tropical Pacific Ocean. *Marine Science*
940 *Bulletin, 12(5)*,211-25,1993.
941 Yang, S., K. M. Lau, and K. M. Kim: Variations of the East Asian jet stream and
942 Asian-Pacific-American winter climate anomalies, J. Climate, 15,306–325 , 2002.
943 Yang Se-Hwan and Lu Riyu: Predictability of the East Asian winter monsoon indices by the coupled
944 models of ENSEMBLES, Advances in Atmospheric Sciences, 31(6), 1279–1292, 2014
945 Yim SY, Wang B, Kwon M: Interdecadal change of the controlling mechanisms for East Asian early
946 summer rainfall variation around the mid-1990s.ClimDyn., 42,1325–1333, 2013.
947 Yim, S.-Y., B. Wang, W. Xing, M.-M.Lu: Prediction of Meiyu rainfall in Taiwan by multi-lead
948 physicalempiricalmodels.Clim. Dyn., 44 (11-12), 3033-3042, doi:10.1007/s00382-014-2340-0, 2015.
949 Yoon, J., and S. W. Yeh: Influence of the Pacific Decadal Oscillation on the relationship between El
950 Ni˜no and the northeast Asian summer monsoon, J. Climate,23, 4525–4537, 2010.
951 Yu H., J. Huang, and J. Chou: Improvement of Medium-Range Forecasts Using the
952 Analogue-Dynamical Method,Mon. Wea. Rev., 142, 1570–1587, doi:
953 http://dx.doi.org/10.1175/MWR-D-13-00250.1, 2014a.
954 Yu H., J. Huang, W. Li, and G. Feng: Development of the analogue-dynamical method for error
955 correction of numerical forecasts,J. Meteor. Res., 28(5), 934–947, doi: 10.1007/s13351-014-4077-4 ,
956 2014b.
957 Zhang R. and Hong M., et al.: Non-linear Dynamic Model Retrieval of Subtropical High Based on
958 Empirical Orthogonal Function and Genetic Algorithm,Applied Mathematics and
959 Mechanics,27(12),1645-1654, 2006.
960 Zhang R. and Hong M.,et al.: Retrieval of the non-linear dynamic forecast model of El Nino/La Nina
961 index based on the genetic algorithm optimization. Chinese Journal of Geophysics,51(5),1354-1362,
962 2008.
963 Zhang R. H., Zhou G. Q. and Chao J. P.: ENSO Dynamics and Its Prediction,Chinese Journal of
964 Atmospheric Sciences,27(4) ,674-688, 2003a.
965 Zhang, R.H., S. E. Zebiak, R. Kleeman, and N.Keenlyside: A new intermediate coupled model for El

Niño simulation and prediction. Geophys. Res.Lett., 30, doi:10.1029/2003GL018010, 2003b.

Zhang, R. H., A. Sumi, and M. Kimoto: Impact of El Niˆnoon the East Asian monsoon: A diagnostic study of the ’86/87 and ’91/92 events,J. Meteor. Soc. Japan, 74, 49–62, 1996.

Zhang Y. L., Yu Y. Q., Duan W. S.: The spring prediction barrier of ENSO in retrospective prediction experiments as shown by the four coupled ocean-atmosphere models. Acta Meteorologica Sinica, 70(3), 506-519, 2012.

Zhao J. H., Liu X. Y. and Jiang H. Y., et al.: Characteristics of Sea Surface Height in Tropical Pacific and its relationship with ENSO events, Meteorological and Environmental Sciences, 35(2),33-39, 2012.

Zheng C. W., Pan J., Li C. Y.. Global oceanic wind speed trends. Ocean & Coastal Management, 129, 15-24,2016.

Zheng C. W., Wang Q., Li C. Y.. An overview of medium- to long-term predictions of global wave energy resources. Renewable and Sustainable Energy Reviews, 79 , 1492-1502,2017.

Zhou, L.-T., and R. G. Wu: Respective impacts of the East Asian winter monsoon and ENSO on winter rainfall in China,J. Geophys. Res.,115, doi: 10.1029/2009JD012502, 2010.

List of Figures:

Fig.1(a, c) First and second modes of the EOF deconstruction of the SSTA field, and (b, d) the corresponding PC time series.

Fig. 2 Forecast results of the first time coefficient series (a) and the second time coefficient series (b) of the SSTA field by the original model

Fig. 3. The cross-validated retroactive hindcast results of the first time coefficient series (a) and the second time coefficient series (b) of the SSTA field by the original model

Fig. 4. Long-term step-by-step forecast results of the first time coefficient series (a) and the second time coefficient series (b) of the SSTA field by the improved model

Fig. 5. The cross-validated retroactive hindcast results of the first time coefficient series (a) and the second time coefficient series (b) of the SSTA field by the improved model

Fig. 6. The forecast SSTA field (a) and the actual SSTA field (b) of an El Niño event (Dec.1997)

Fig. 7. The forecast SSTA field (a) and the actual SSTA field (b) of a La Niña event (Dec.1999)

Fig. 8. The forecast SSTA field (a) and the actual SSTA field (b) of neutral event (Nov.2002)

Fig. 9. The improved dynamical-statistical model prediction of the ENSO index

Fig. 10. Temporal correlation between model forecasts and observations for all seasons combined, as a function of lead time. Each line highlights one model.

Fig.11. RMSE in standardized units, as a function of lead time for all seasons combined. Each line highlights one model.

Table captions:

Table 1. The correlation analysis between the front two time series T_1, T_2 and nine impact factors

Table2. The CC and MAPE of long-term fitting test when the retrospective order p is different

Table3. The forecast results of T_1 and T_2 in different examples within 6 and 12 months

Table. 4. The TC and the MAPE between model forecasts and observations within 12 months for Nov.–Jan., Dec.–Feb., and Jan.–Mar. as lead time of winter, for Feb.–Apr. , Mar.–May and Apr.–June as lead time of spring, for May-July, June-August and July-Sep. as lead time of summer and for August-Oct., Sep.-Nov. and Oct.-Dec. as lead time of autumn.

Figure:

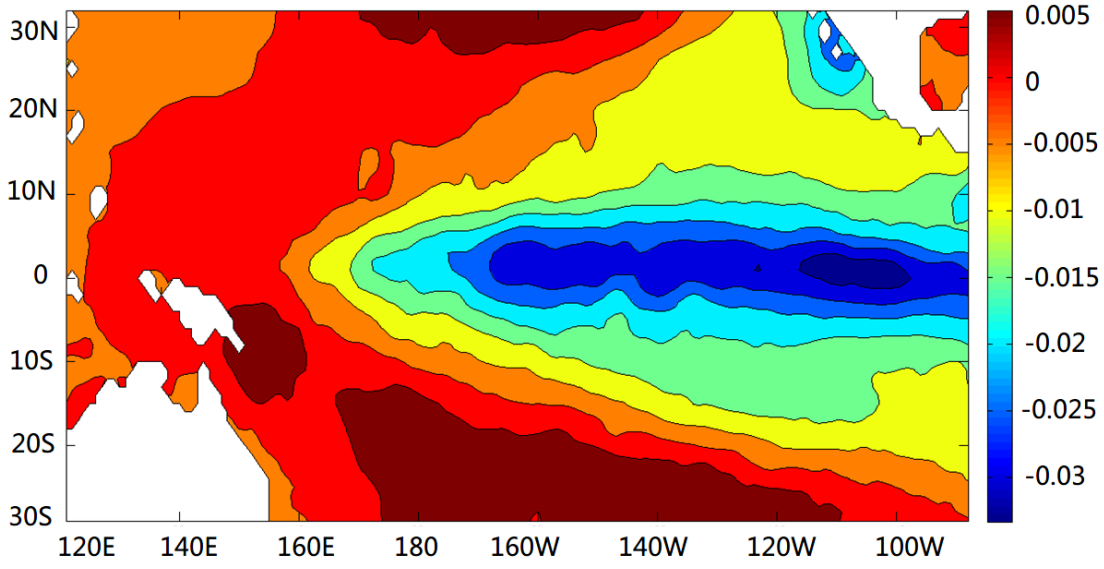
30N
20N
10N
0
10S
20S
30S
120E
140E
160E
180
160W
140W
120W
100W
0.005
0
-0.005
-0.01
-0.015
-0.02
-0.025
-0.03

(a)

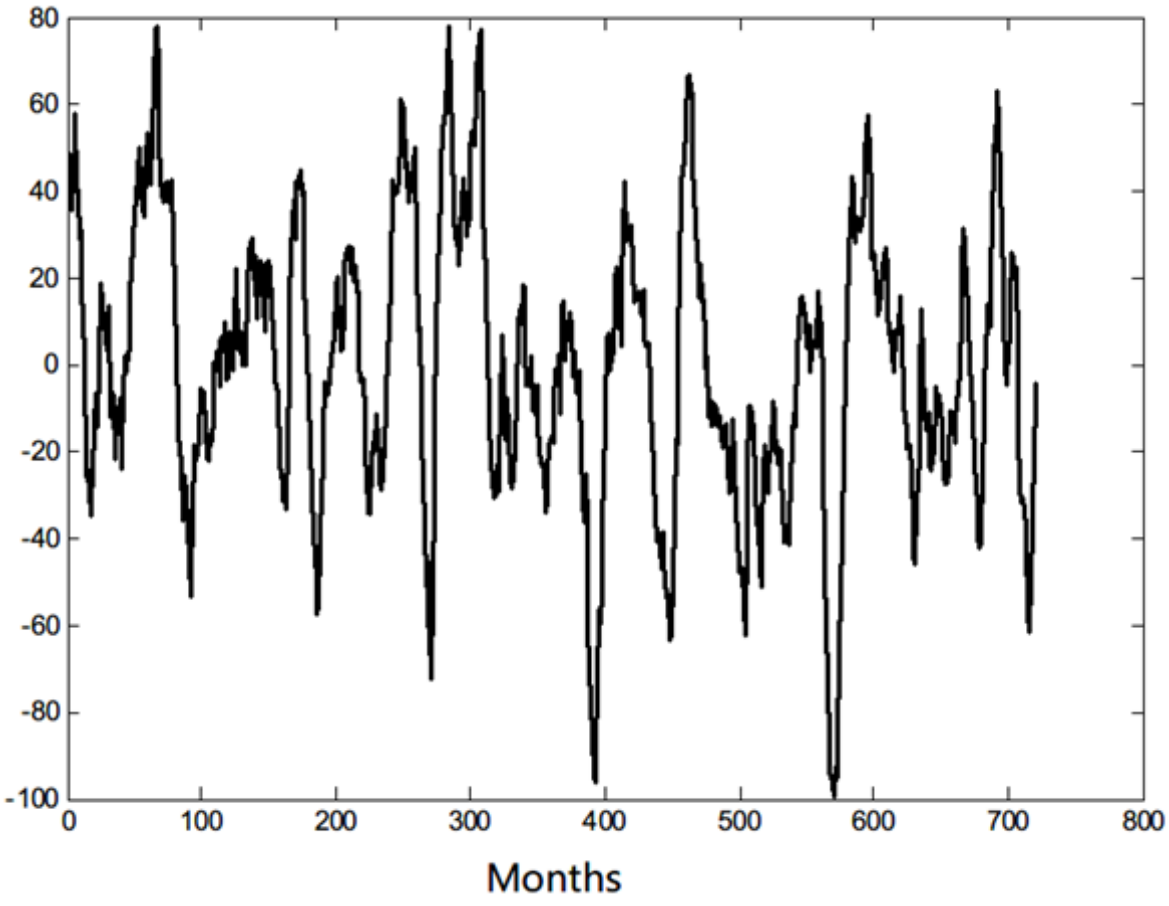
80
60
40
20
0
-20
-40
-60
-80
-100
0
100
200
300
400
500
600
700
800
Months

(b)

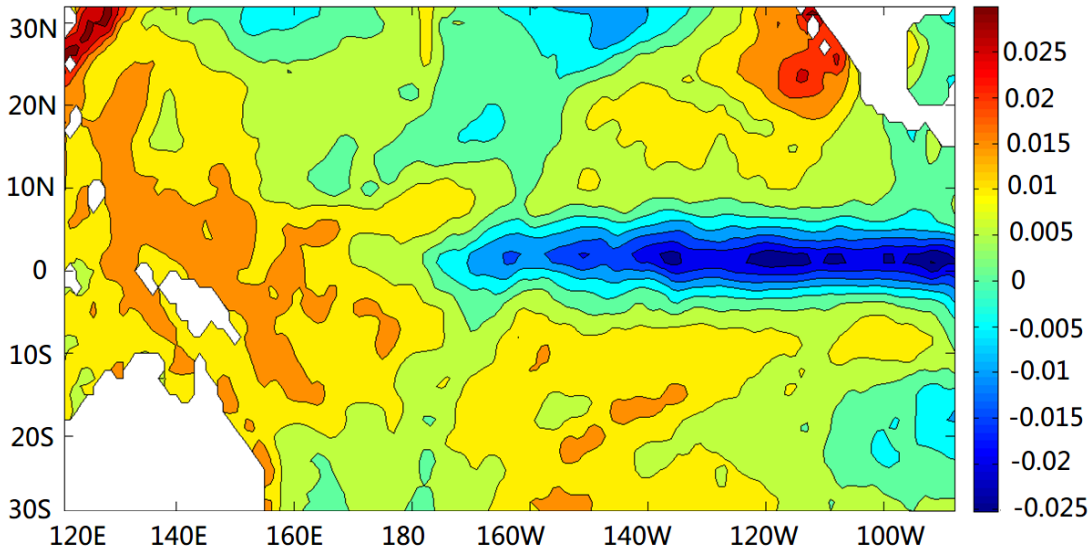

(c)

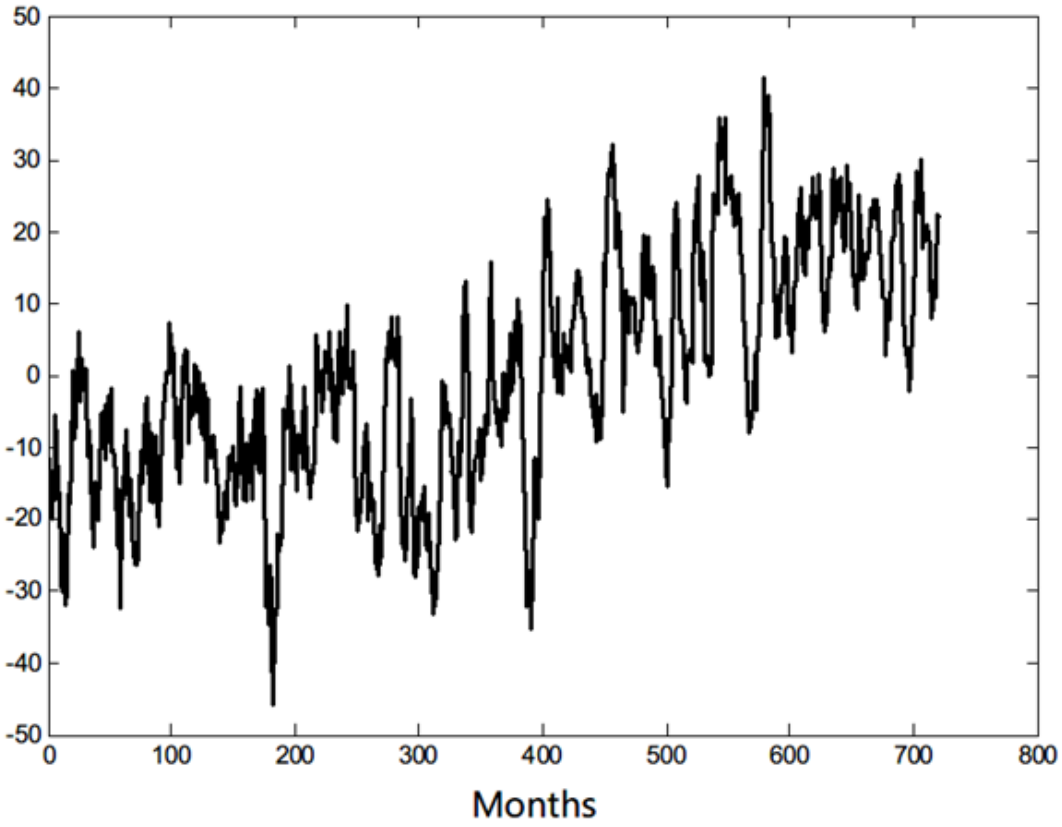

(d)

Fig. 1 (a, c) First and second modes of the EOF deconstruction of the SSTA field, and (b, d) the corresponding PC time series.

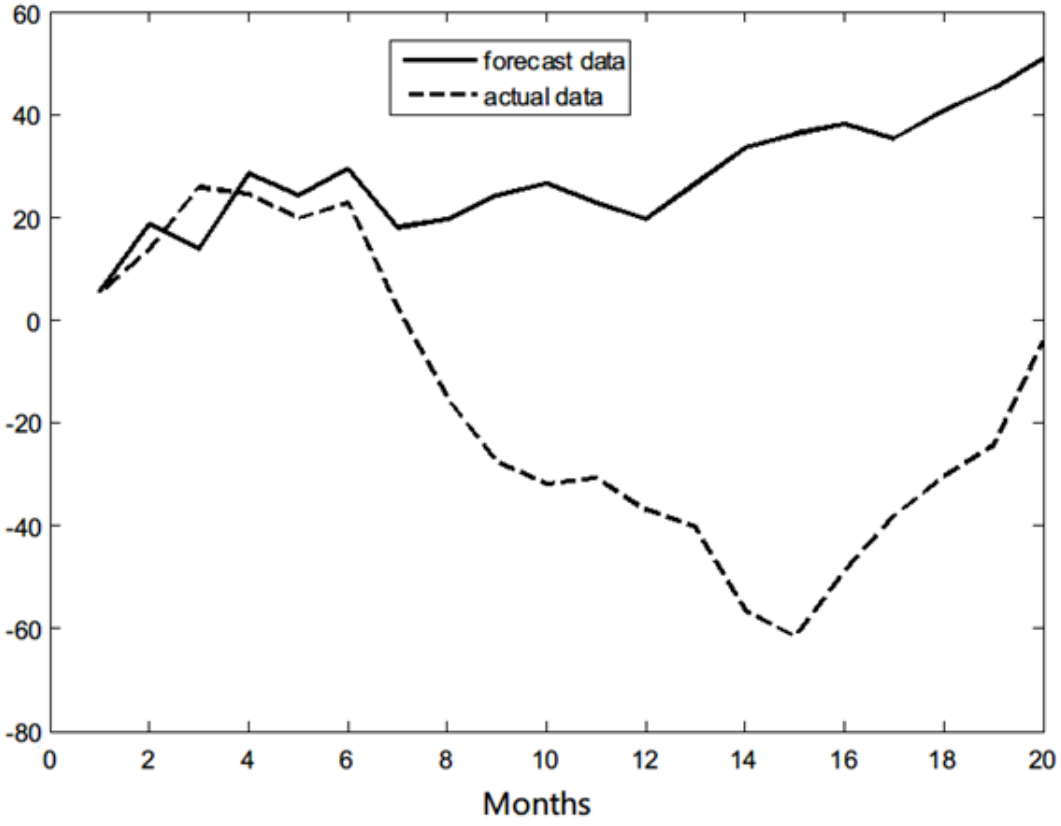

1049

1050 (a)

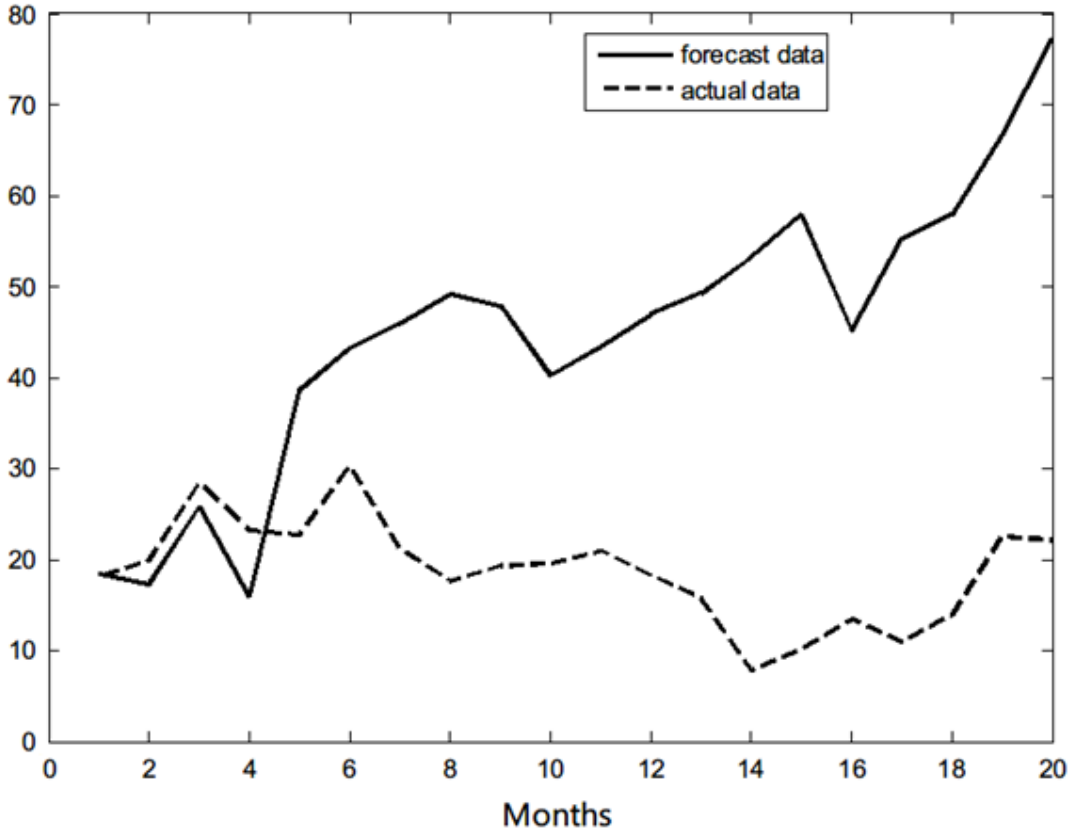

1051

(b)

Fig.2 Forecast results of the first time coefficient series T_1 (a) and the second time coefficient series T_2 (b)of the SSTA field by the original model

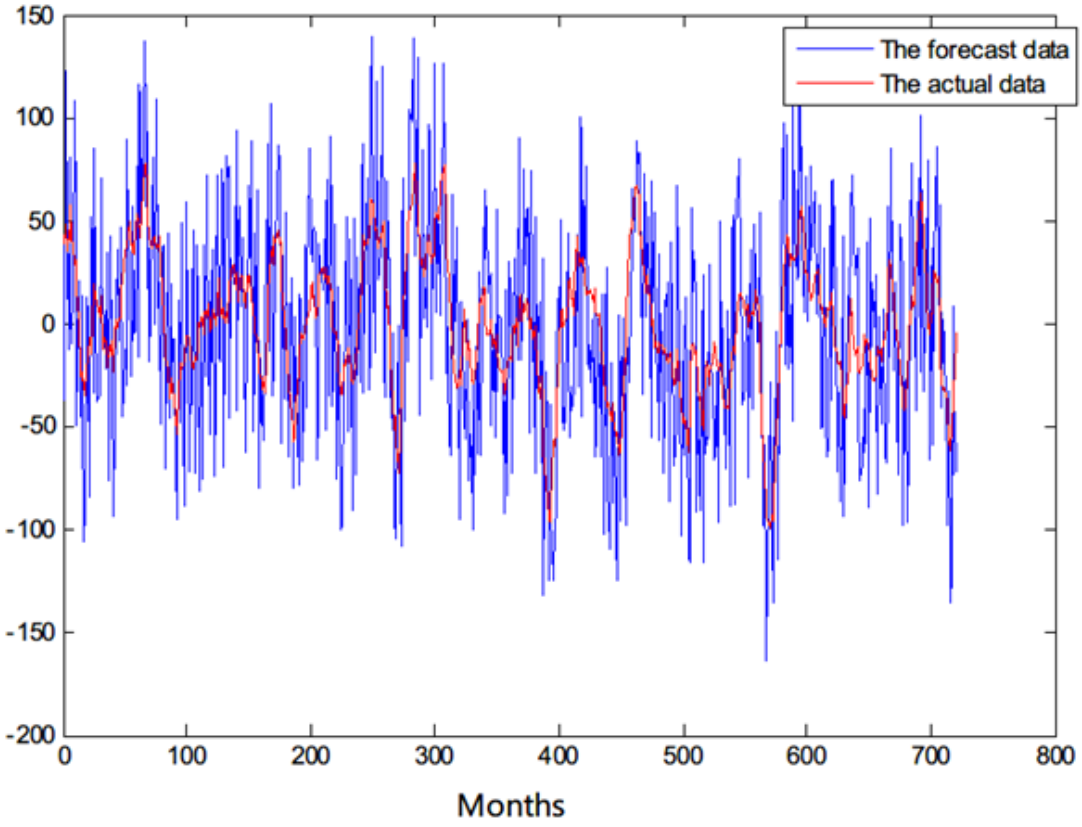

1066

1067 (a)

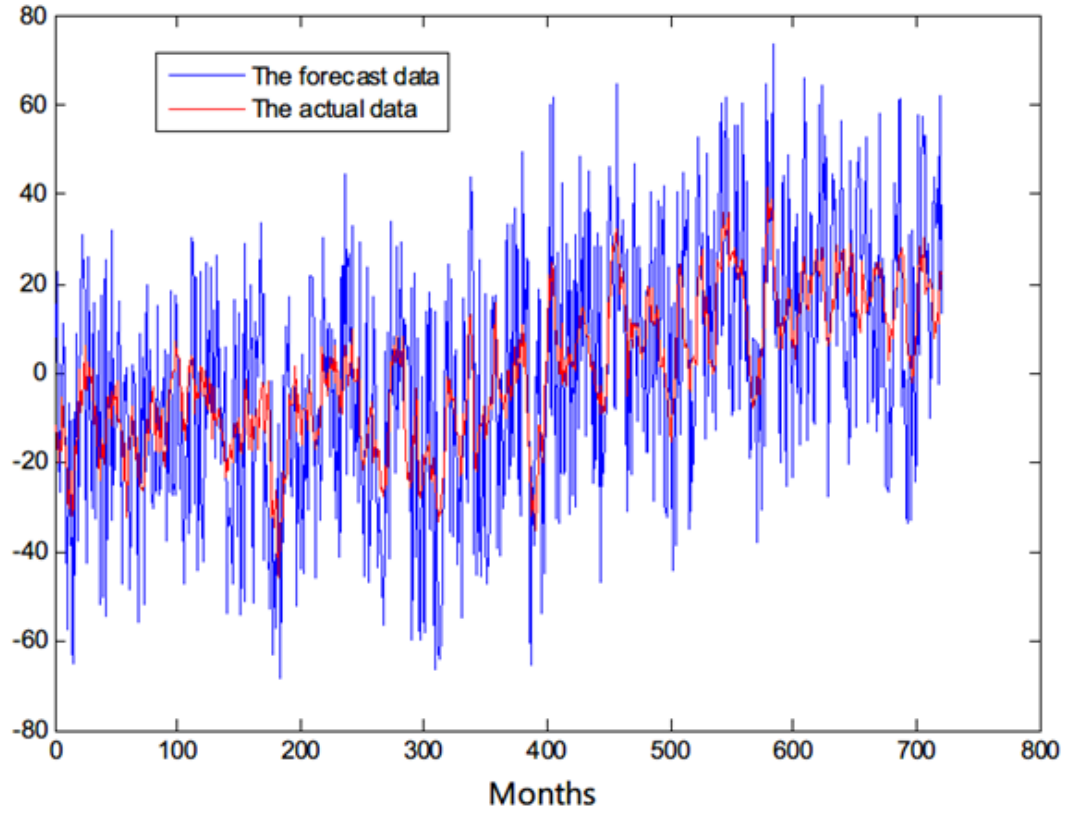

1068

(b)

Fig.3The cross-validated retroactive hindcast results of the first time coefficient series T_1 (a)and the second time coefficient series T_2 (b)of the SSTA field by the original model

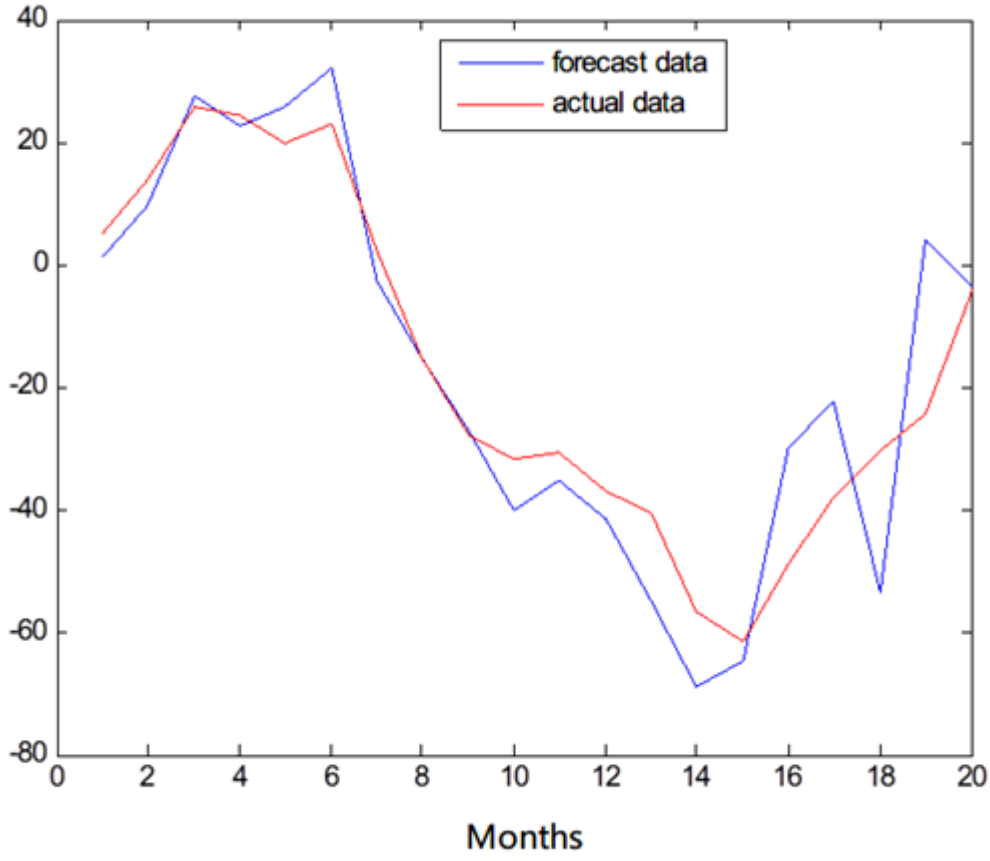
forecast data
actual data
40
20
0
-20
-40
-60
-80
0
2
4
6
8
10
12
14
16
18
20
Months

1081

1082 (a)

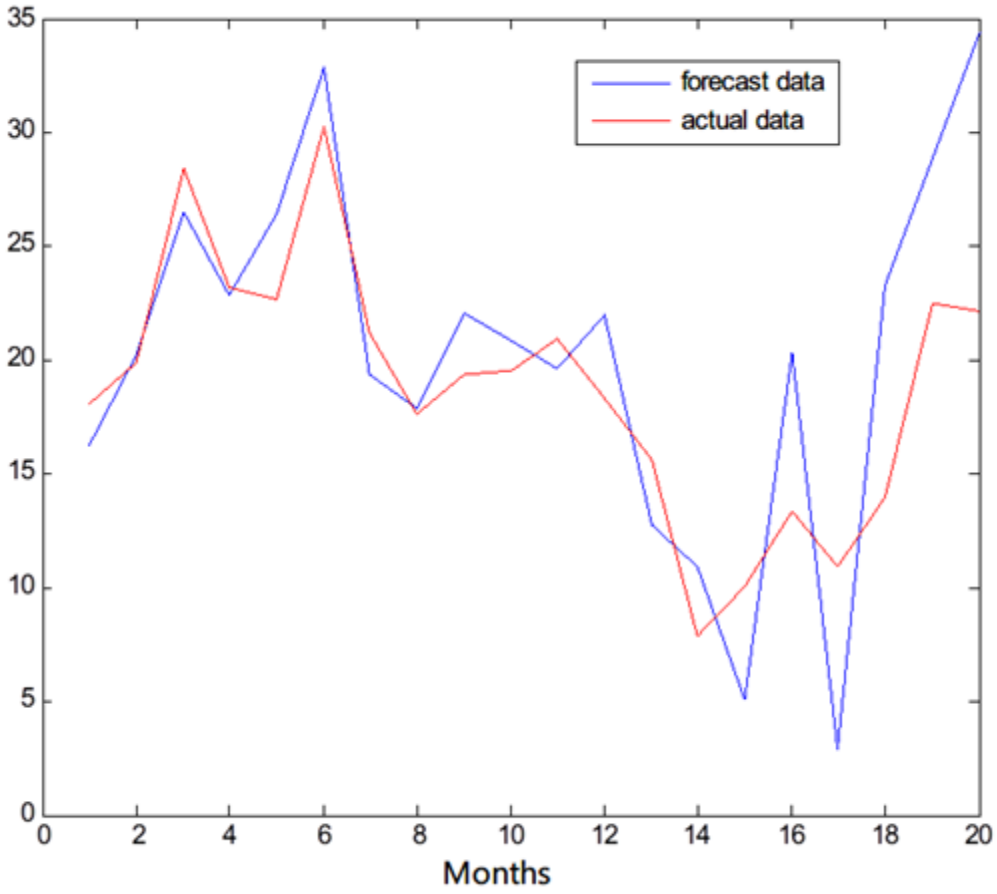

(b)

Fig. 4. Long-term step-by-step forecast results of the first time coefficient series T_1 (a)and the second time coefficient series T_2 (b)of the SSTA field by the improved model

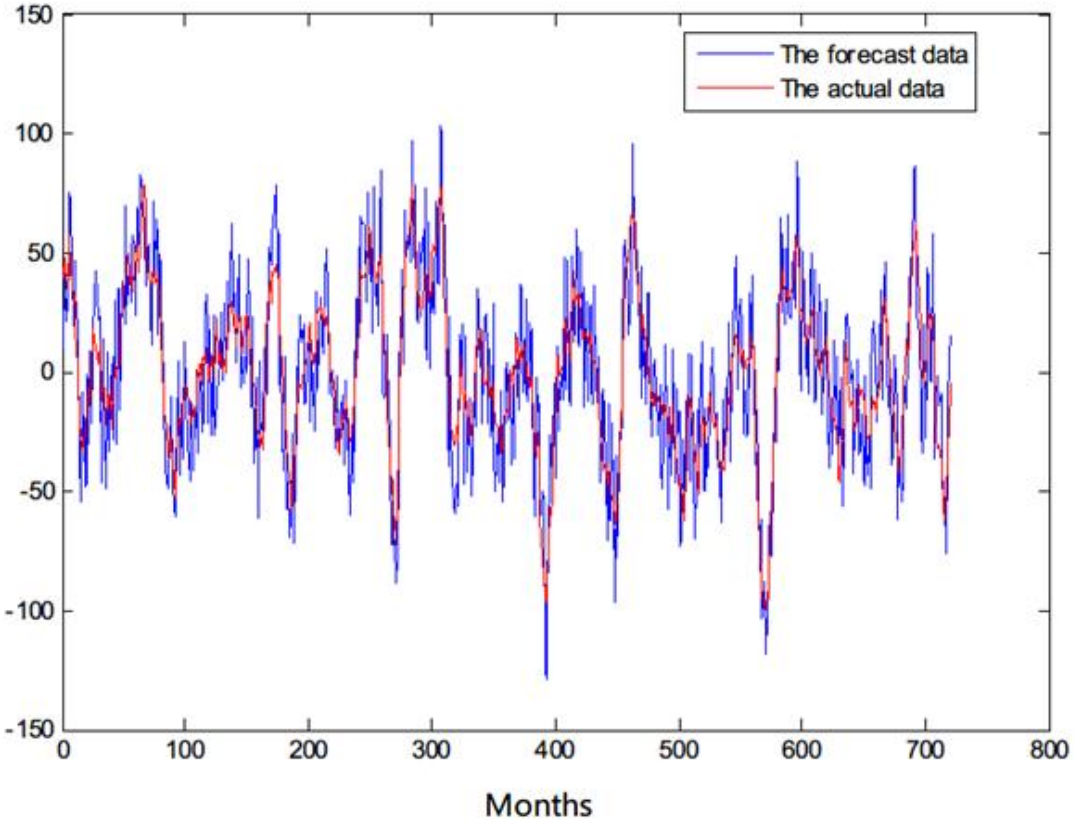
The forecast data
The actual data
150
100
50
0
-50
-100
-150
0
100
200
300
400
500
600
700
800
Months

(a)

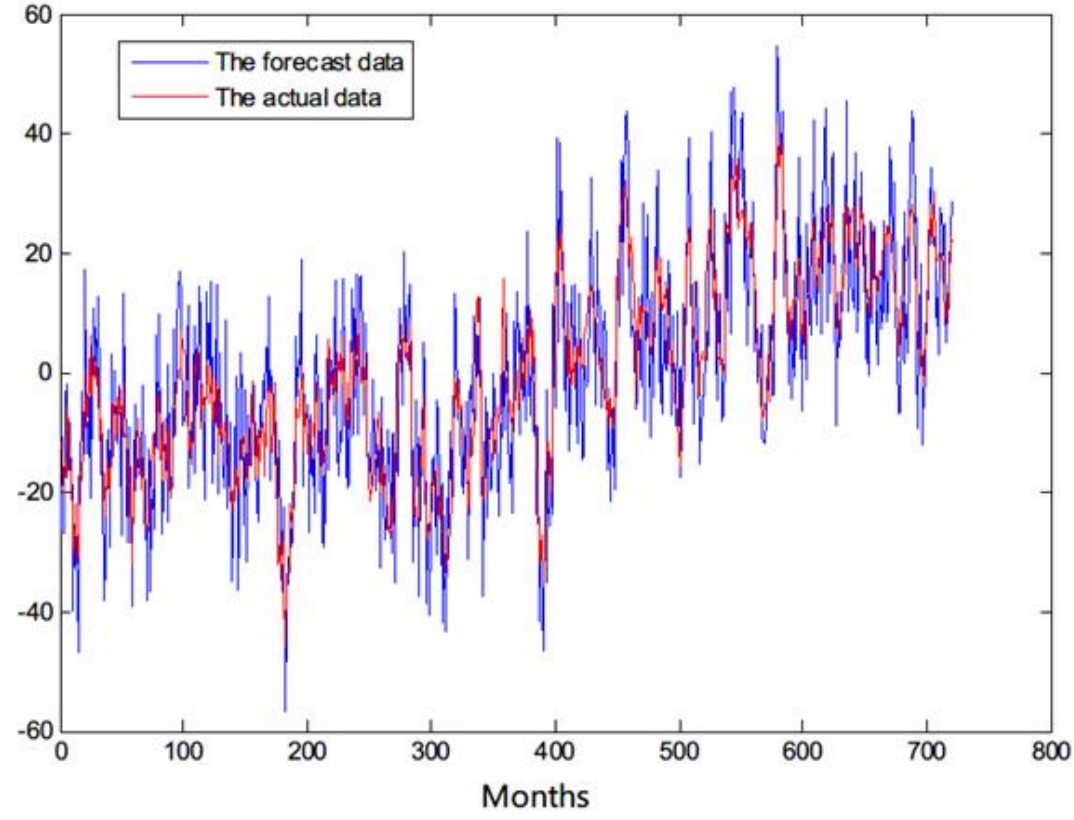
The forecast data
The actual data
60
40
20
0
-20
-40
-60
0
100
200
300
400
500
600
700
800
Months

(b)

Fig. 5. The cross-validated retroactive hindcast results of the first time coefficient series T_1 (a)and the second time coefficient series T_2 (b)of the SSTA field by the improved model

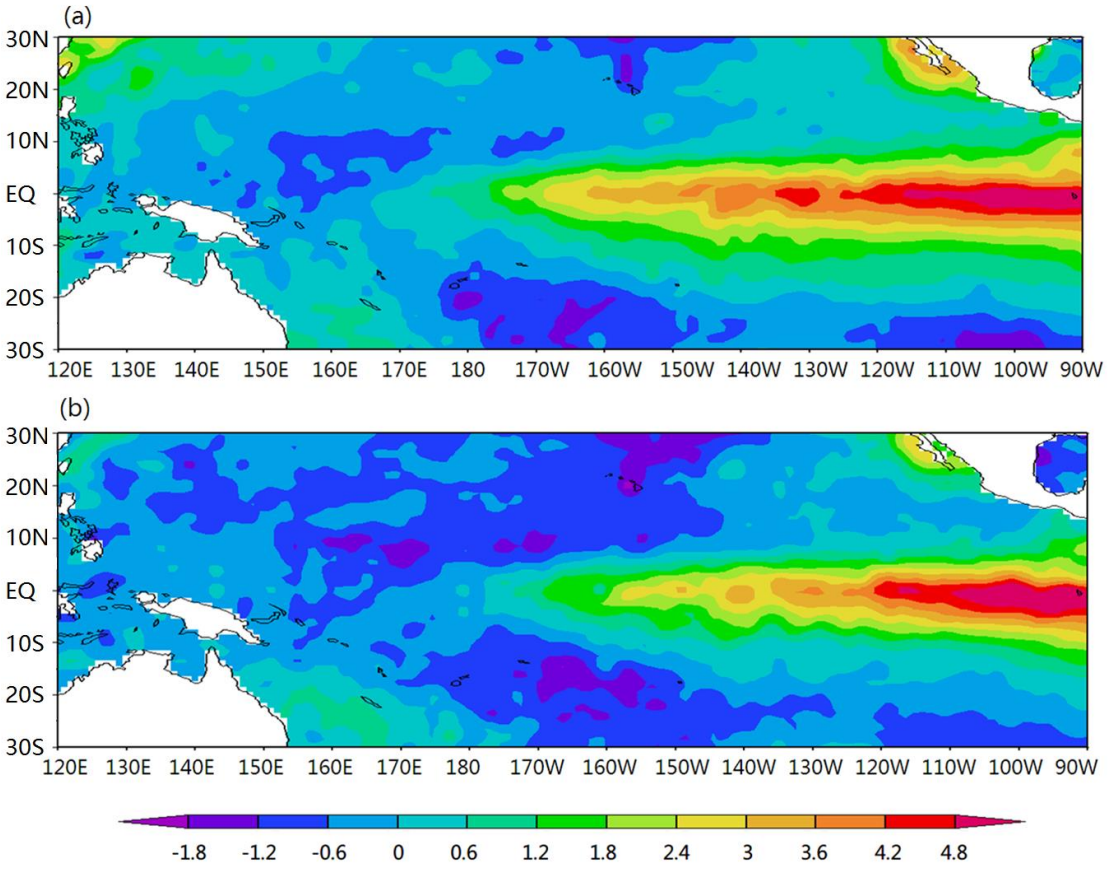

1102

1103 Fig.6. The forecast SSTA field(a) and the actual SSTA field (b)of an El Niño event (Dec.1997)

1104

1105

1106

1107

1108

1109

1110

1111

1112

1113

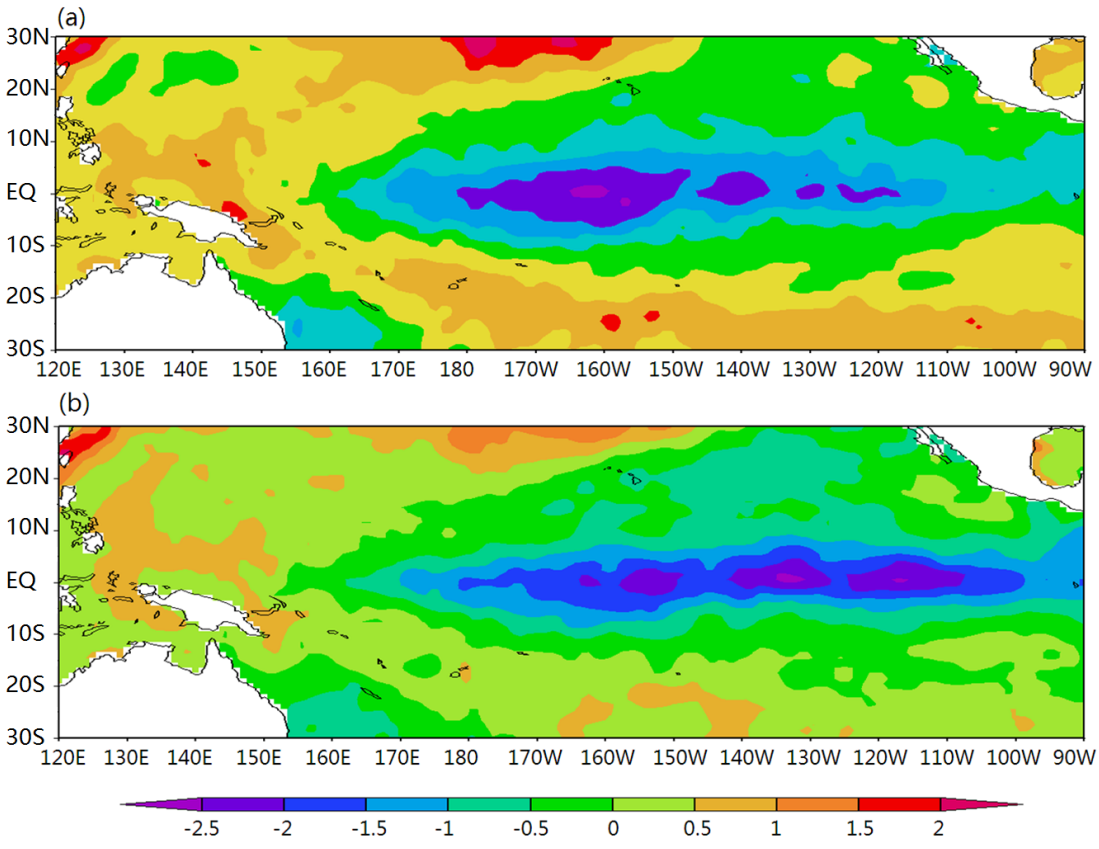

1114

1115 Fig.7. The forecast SSTA field(a) and the actual SSTA field (b)of a La Niña event (Dec.1999)

1116

1117

1118

1119

1120

1121

1122

1123

1124

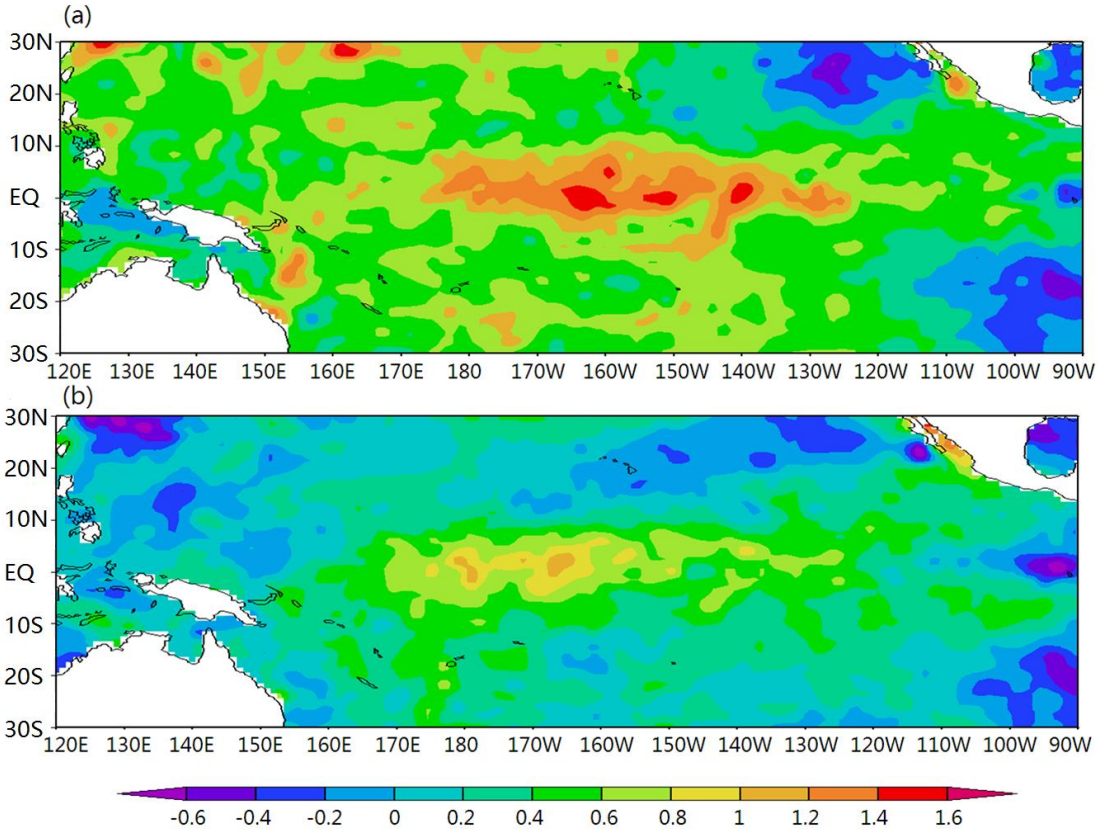

1125

1126 Fig.8. The forecast SSTA field(a) and the actual SSTA field (b)of neutral event (Nov.2002)

1127

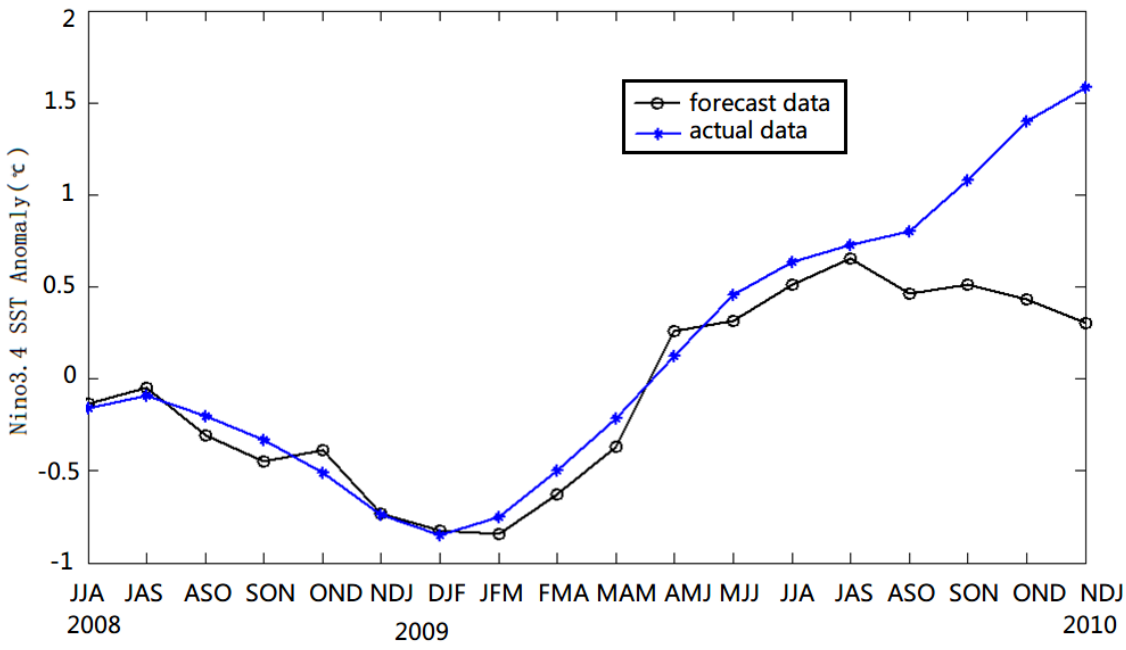

Fig.9. The improved dynamical-statistical model prediction of the ENSO index

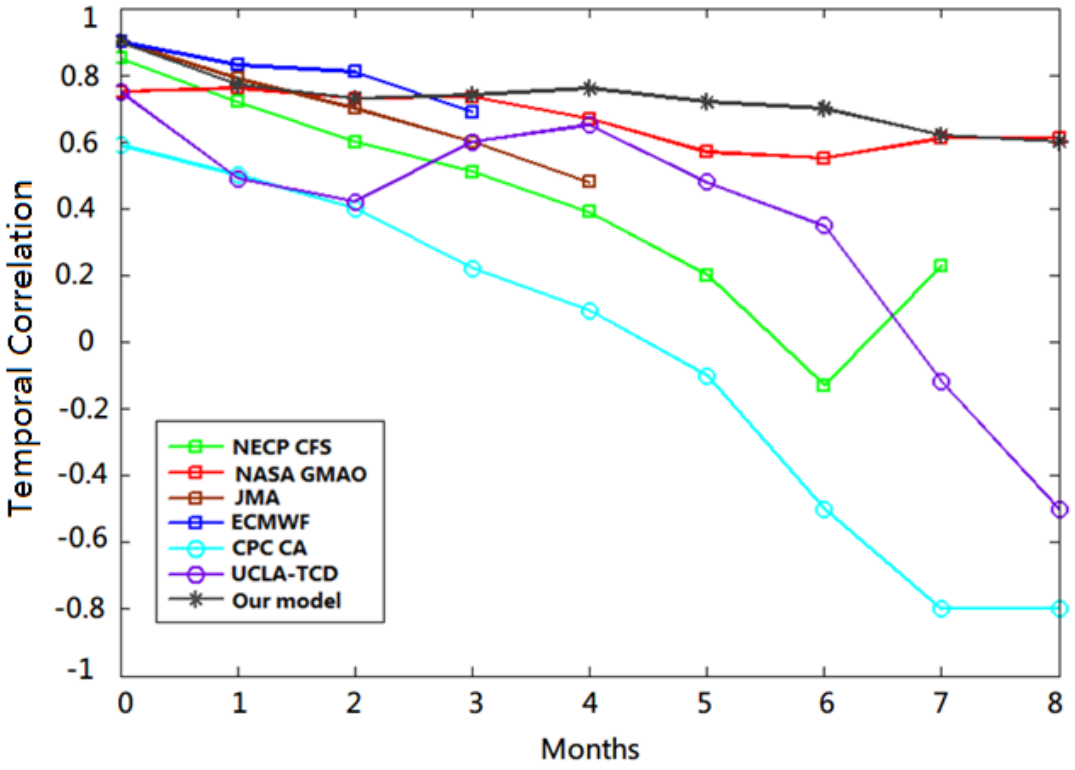

Fig. 10. Temporal correlation between model forecasts and observations for all seasons combined, as a function of lead time. Each line highlights one model.

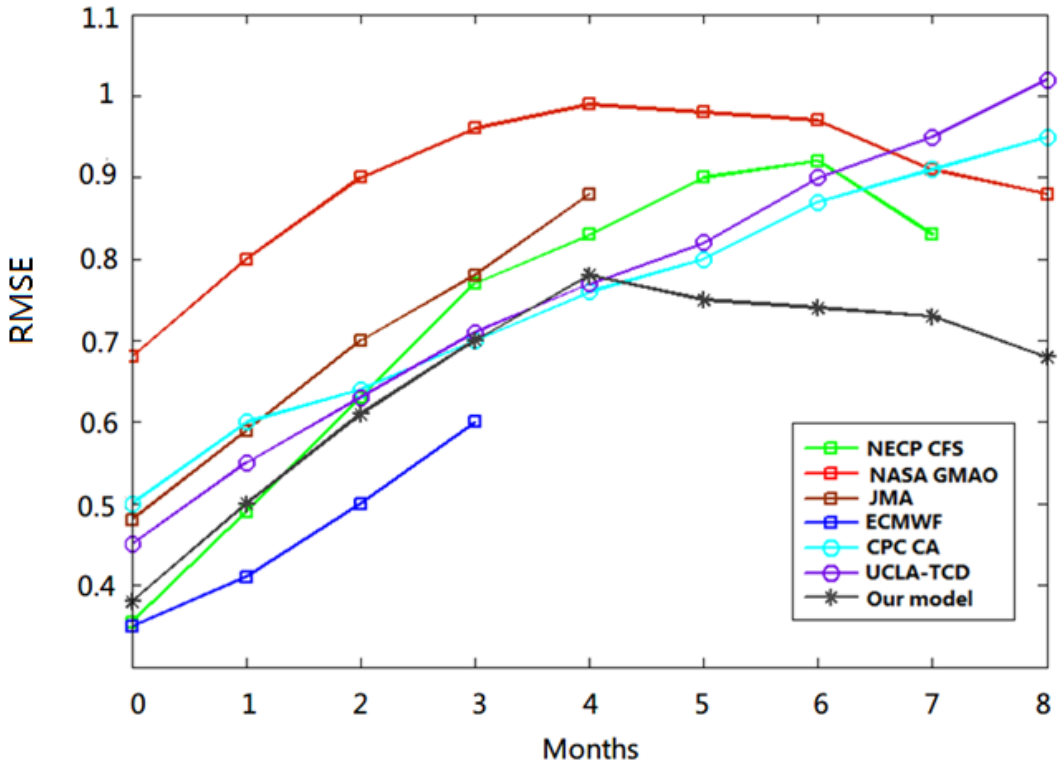

Fig . 11. RMSE in standardized units, as a function of lead time for all seasons combined. Each line highlights one model.

Table:

Table 1. The correlation analysis between the front two time series T_1, T_2 and nine impact factors

factors	u_1	u_2	PNA	DMI	SOI	PDOI	EAWMI	OLR	SSH
T_1	0.3161	0.5684	0.4386	-0.3457	0.7734	0.4081	0.6284	0.3287	0.3363
T_2	0.2118	0.4181	0.2560	-0.2345	0.5232	0.3065	0.4825	0.1816	0.2169

Table2. The CC and MAPE of long-term fitting test when the retrospective order p is different

p		4	5	6	7	8	9	10
The forecast results of long-term fitting test	CC	0.75	0.73	0.81	0.74	0.70	0.72	0.68
	MAPE	18.42%	19.36%	14.56%	20.39%	25.31%	24.18%	27.33%
p		11	12	13	14	15	16	
The forecast results of long-term fitting test	CC	0.68	0.70	0.65	0.62	0.60	0.62	
	MAPE	28.10%	26.58%	30.91%	33.14%	34.97%	33.56%	

1223 **Table3.** The forecast results of T_1 and T_2 in different examples within 6 and 12 months

1224

Forecast events	The results within 6-months		The results within 12-months	
	CC	MAPE	CC	MAPE
The average of 18 El Niño examples of T_1	0.824	8.45%	0.719	12.67%
The average of 22 La Niña examples of T_1	0.846	7.68%	0.740	11.28%
The average of 20 Neutral examples of T_1	0.885	6.23%	0.789	9.85%
The average of total 60 examples of T_1	0.850	7.41%	0.748	10.95%
The average of 18 El Niño examples of T_2	0.811	8.79%	0.703	13.28%
The average of 22 La Niña examples of T_2	0.833	7.35%	0.731	11.96%
The average of 20 Neutral examples of T_2	0.896	6.68%	0.795	10.08%
The average of total 60 examples of T_2	0.842	7.64%	0.740	11.71%

1225

1226

1227

1228

1229

1230

1231

1232

1233

Table. 4. The TC and the MAPE between model forecasts and observations within 12 months for Nov.–Jan., Dec.–Feb., and Jan.–Mar. as lead time of winter, for Feb.–Apr. , Mar.–May and Apr.–June as lead time of spring, for May-July, June-August and July-Sep. as lead time of summer and for August-Oct., Sep.-Nov. and Oct.-Dec. as lead time of autumn.

Forecast events	Lead time of all seasons combined		Lead time of summer (MJJ-JJA-JAS)		Lead time of autumn (ASO-SON-OND)		Lead time of winter (NDJ-DJF-JFM)		Lead time of spring (FMA-MAM-AMJ)	
	TC	MAPE	TC	MAPE	TC	MAPE	TC	MAPE	TC	MAPE
The average of 18 El Niño examples	0.604	9.70%	0.569	10.33%	0.632	8.85%	0.677	8.02%	0.538	11.6%
The average of 22 La Niña examples	0.625	8.97%	0.581	9.82%	0.645	8.41%	0.695	7.83%	0.579	9.82%
The average of 20 Neutral examples	0.798	5.96%	0.752	6.86%	0.831	5.31%	0.844	4.60%	0.765	7.07%
The average of total 60 examples	0.712	7.62%	0.633	8.51%	0.786	6.88%	0.776	6.52%	0.653	8.03%